A 3D layer-wise model for the correct imposition of transverse shear/normal load conditions in FGM shells

A 3D layer-wise model for the correct imposition of transverse shear/normal load conditions in FGM shells

Salvatore Brischetto*

Abstract *A general elasticity 3D layer-wise shell model is proposed for the static investigation plates and shells including functionally graded material (FGM) layers. A closed-form solution is used considering simply-supported sides and harmonic forms for displacements and loads. The partial differential equations obtained from the 3D equilibrium relations developed in curvilinear orthogonal coordinates are solved using the exponential matrix methodology. These equations have constant coefficients because an opportune number of mathematical layers has been introduced in order to calculate the parametric coefficients including the radii of curvature for the shells and the elastic coefficients that are variable through the thickness direction in the case of functionally graded materials. The main aim of the present work is to fill the gap found in the literature where the 3D elasticity theories always give solutions for FGM plates or shells in the only case of a transverse normal load positioned at the top or at the bottom surfaces. The present work proposes an exhaustive static analysis where the load boundary conditions have been appropriately rewritten in order to allow the use of several transverse normal and transverse shear loads separately or simultaneously positioned at top and/or bottom surfaces. One-layered and sandwich FGM plates, cylinders, cylindrical shells and spherical shells are analyzed changing the material laws and properties, the applied loads and the thickness ratios. The importance of the zigzag features, the interlaminar continuity in terms of compatibility and equilibrium requirements, the boundary load requirements, the considerations about the symmetry, the thickness ratio effect and the three-dimensional behavior have been opportunely discussed. Advantages connected with the use of FGM layers have also been analyzed. These new 3D exact results will allow the validation of recent advanced 2D shell models in the literature for the static investigation of FGM structures subjected to different load conditions. The proposed 3D model is general for several geometries (plates and shells) and materials (classical ones, composites and FGMs) and it allows a unique 3D exact solution for a large variety of structures.*

Keywords: general 3D shell model, functionally graded materials, plates and shells, transverse shear and transverse normal loads, layer-wise method, exponential matrix solution.

1 Introduction

Functionally graded materials (FGMs) are recent advanced materials designed for specific performances and functions in the engineering field. The spatial gradation in structure and/or composition allows tailored properties. FGMs have a specific spatial distribution of the constituent phases (such as metals, ceramics and polymers) with a continuous variation in composition. The major advantages of FGMs in comparison with other composites are physical and mechanical gradients in specific directions in order

*DIMEAS - Department of Mechanical and Aerospace Engineering, Politecnico di Torino, corso Duca degli Abruzzi, 24, 10129 Torino, ITALY. e.mail: salvatore.brischetto@polito.it, tel: +39.011.090.6813, fax: +39.011.090.6899.

to achieve tailored morphologies [1]. Advanced aerospace structures require multi-function materials. FGMs possess this feature because several contrasting functions are incorporated into a single material (e.g., toughness of the polymeric materials or important mechanical properties of metallic materials combined with the temperature capability of the ceramics). FGMs here considered have continuous change in composition and microstructure across the thickness direction. In the case of sandwiches, the two external surfaces have in general the pure composition of the two components of the FGM [2]. The monotonous change of the volume fraction of the constituent phases has the advantage of eliminating the physical interfaces which are typical of conventional multilayered structures. In this way, the stress discontinuity is eliminated and delamination-related problems are suppressed [3]. FGMs are extensively employed in aerospace, automotive, marine and biomedical fields because of high thermal properties and fracture toughness, and reduced stress intensity factors and residual stress distributions [4], [5].

In engineering applications, structures embedding FGM layers are correctly designed after an accurate evaluation of strains, stresses, displacements, vibrations and modes. In order to perform satisfactory analyses, 3D, 2D and 1D models can be applied. In the literature, a large amount of 3D, 2D and 1D models have been extended to FGM structures in analytical or numerical form. 3D analytical models are in general employed to produce assessment results for the validation of 3D numerical or refined 2D numerical/analytical models. 3D numerical models are used for the analysis of structures with particular geometrical, thickness and material properties that make impossible their investigation by means of 2D or 1D models. 3D models found in the literature can be analytical, numerical or semi-analytical. They have been extended to FGM structures for free vibration, dynamic and static analyses (also including mechanical, thermal and electrical loads). The 3D exact model by Hosseini-Hashemi et al. [6] was used for the free vibration analysis of plates including FGM layers. In this case, the elasticity modulus and mass density of the functionally graded coating were assumed to vary exponentially through the thickness of the layer. Vel and Batra [7] proposed free and forced vibration investigation of simply-supported plates embedding FGM layers by means of an exact 3D plate theory. Results were proposed for two-constituent metal-ceramic functionally graded rectangular plates that had a through-the-thickness power-law for the volume fractions of the constituents. The 3D plate model by Dong [8] was developed, using the Chebyshev-Ritz method, to investigate the free vibrations of annular FGM plates. Two through-the-thickness variation types for material properties were analyzed. The Chebyshev-Ritz method was also employed by Li et al. [9] to analyze the free frequency response of sandwich plates including FGM layers. Two possibilities were investigated, FGM skins and homogeneous core or homogeneous skins and FGM core. The differential quadrature method (DQM) was employed by Malekzadeh [10] for a free frequency plate solution for the analysis of functionally graded structures based on elastic foundation with two parameters. The material properties continuously change through the thickness direction (power law, exponentially law or any other formulation). Alibeigloo et al. [11] developed an analytical 3D shell solution for the free frequency analysis of simply-supported functionally graded piezoelectric cylindrical panels and a semi-analytical 3D shell solution for the free frequency investigation of cylindrical panels embedding piezoelectric functionally graded layers. Material properties vary along the thickness direction by means of an exponential law with constant Poisson ratio. Zahedinejad et al. [12] solved governing equations using trigonometric functions. This proposed 3D numerical shell model was based on the 3D elasticity theory and the differential quadrature method. The model was used for the free vibration investigation of thick shells including FGM layers. Panels had two opposite simply supported edges and arbitrary boundary conditions for the other two edges. Chen et al. [13] investigated the free vibrations of functionally graded shells, including fluid and with variable thickness, by means of a laminated approach suitable for an arbitrary variation of material constants along the radial direction. Vel [14] analyzed free and forced frequencies of functionally graded cylindrical shells using a three-dimensional elasticity model. The investigated shells had simply supported edges and arbitrary material gradation in the radial direction. Sladek et al. [15]- [17] developed a meshless numerical model for the 3D elasticity investigation of functionally

graded bodies. The method was based on the local Petrov-Galerkin theory. The bending analysis of FGM plates was proposed by Xu and Zhou [18] using a 3D theory based on a generalization for displacements and stresses. Young modulus was functionally graded through the thickness direction in accordance with the exponential-law and Poisson ratio was considered as constant. Functionally graded piezoelectric structures was analyzed by Zhong and Shang [19] by means on an exact 3D plate model based on the state space method. Both mechanical and electric properties had the same exponent-law through the thickness direction. Kashtalyan [20] elaborated a three-dimensional plate theory for the static analysis of one-layered FGM structures. The Young modulus varied exponentially through the thickness, and the Poisson ratio was assumed to be constant. This model was extended to the 3D static analysis of sandwich plates embedding FGM layers by Kashtalyan and Menshykova [21]. In order to increase the resistance of sandwich plates to delamination, the concept of a functionally graded material (FGM) core was employed. The static analysis of viscoelastic cylindrical FGM panels was proposed in [22] where a 3D elasticity theory was combined with the state space method and Fourier expansion for simply supported sides. The state space differential quadrature solution was employed for other different boundary conditions. Effects of relaxation time constant, boundary conditions, mid-radius to thickness ratio and power law index on bending behavior of viscoelastic cylindrical panels were investigated. Yang et al. [23] investigated the axisymmetric bending of novel functionally graded polymer nanocomposite circular and annular plates reinforced with graphene nanoplatelets (GPL). The three-dimensional elasticity theory and the general Mian and Spencer methodology were employed. A parametric study was conducted to examine the effects of GPL weight fraction, distribution pattern, plate thickness to radius ratio and boundary conditions. Alibeigloo [24] used the generalized coupled thermoelasticity for the time dependent response of sandwich plates with functionally graded material core. Governing partial differential thermoelasticity equations were reduced to ordinary differential equations by applying Fourier series state space technique and then were analytically solved via Laplace transformation. A 3D analytical solution was elaborated for a longitudinally functionally graded plate in the case of to Levy-type boundary conditions in [25]. The material compliances linearly varied along the x in-plane direction in each single layer. Further interesting works about functionally graded structures, in particular cylindrical shells, can be found in [26]- [28] where new applications and methods were discussed.

The 3D analytical and numerical models for FGM structures proposed in the investigated literature have the main limitation of investigating only defined geometries that are plate or shell geometries in a separated formulation. The present model for FGM structures is a general formulation valid for simply supported spherical shells. It considers plates, cylinders and cylindrical shells as particular cases. In this way, a general and unique tool has been developed for different geometries. The static analysis proposed in the present work considers transverse normal/shear loads that can be applied simultaneously or separately at both top and/or bottom external surfaces in harmonic form. For all these reasons, the developed 3D exact shell model for FGM structures can be considered as one of the most general and complete theories in the literature. The author proposed in [29] the 3D exact static analysis of multilayered composite and sandwich plates and shells when transverse normal loads were positioned at the external surfaces. This model was extended to the static analysis of functionally graded plates and shells in [30]. Paper [31] modified the boundary loading conditions in order to introduce combinations of transverse normal and transverse shear loads at the external surfaces for the cases analyzed in [29]. The present new work introduces these new boundary load conditions in the static analysis of functionally graded plates and shells in order to apply transverse shear/normal loads in the FGM benchmarks already proposed in [30]. The present model is a layer-wise 3D exact theory based on the differential equations of equilibrium written in general orthogonal curvilinear coordinates. These equations are valid for spherical and cylindrical shells, cylinders and plates. The system of partial differential equations are solved using of the exponential matrix solution [32]- [35]. This method was used by Messina [36] for the 3D free vibration analysis of composite plates using equilibrium equations

written in orthogonal rectilinear coordinates. Soldatos and Ye [37] employed the exponential matrix method to solve the three-dimensional equilibrium relations developed in cylindrical coordinates for the free vibration investigation of multilayered composite cylinders. The three-dimensional model by Fan and Zhang [38] allows free frequency and bending investigation of composite spherical panels. The exponential matrix methodology was used for the solution of 3D equilibrium relations. Deep spherical and shallow spherical shells were analyzed. Plates were considered as very shallow spherical shells. In [38], cylindrical shell, cylinder and plate cases were not investigated. Fan and Zhang [38] developed a theory where the displacements and the transverse stresses are the six main variables of the model. The Cayley-Hamilton procedure was applied. The new model of the present author considers displacements and their derivatives in z as the six main variables of the model. The different approach here employed allows a large number of mathematical layers that permits the analysis of very thick shells and the extension to functionally graded plates and shells. The model here proposed was also used in the past by the author for the free vibration analysis of one-layered [39] and multilayered composite and sandwich [40] structures and for mode analysis of functionally graded plates and shells [41]. The convergence analysis of the method in terms of order of expansion for the exponential matrix and number of mathematical layers was already proposed in [42] and [43].

The layer-wise 3D shell model is presented in Section 2. Section 3 shows the main results. The first part of this section is devoted to the preliminary assessments in order to validate the model; the second part proposes the new benchmarks for the new load conditions. Finally, Section 4 gives the main conclusions and considerations.

2 Layer-wise 3D shell model

The compact form of constitutive relations for a generic functionally graded material (FGM) layer k is:

$$\boldsymbol{\sigma}^k = \boldsymbol{C}^k(z)\boldsymbol{\epsilon}^k \,, \tag{1}$$

where the stress components are included in $\boldsymbol{\sigma}^k = \{\sigma^k_{\alpha\alpha}\, \sigma^k_{\beta\beta}\, \sigma^k_{zz}\, \sigma^k_{\beta z}\, \sigma^k_{\alpha z}\, \sigma^k_{\alpha\beta}\}^T$ and the strain components are in $\boldsymbol{\epsilon}^k = \{\epsilon^k_{\alpha\alpha}\, \epsilon^k_{\beta\beta}\, \epsilon^k_{zz}\, \gamma^k_{\beta z}\, \gamma^k_{\alpha z}\, \gamma^k_{\alpha\beta}\}^T$. T means the transpose of a vector. The 6×6 elastic coefficient matrix $\boldsymbol{C}^k(z)$ considered for the k isotropic functionally graded material layer is:

$$\boldsymbol{C}^k(z) = \begin{bmatrix} C^k_{11}(z) & C^k_{12}(z) & C^k_{13}(z) & 0 & 0 & 0 \\ C^k_{12}(z) & C^k_{22}(z) & C^k_{23}(z) & 0 & 0 & 0 \\ C^k_{13}(z) & C^k_{23}(z) & C^k_{33}(z) & 0 & 0 & 0 \\ 0 & 0 & 0 & C^k_{44}(z) & 0 & 0 \\ 0 & 0 & 0 & 0 & C^k_{55}(z) & 0 \\ 0 & 0 & 0 & 0 & 0 & C^k_{66}(z) \end{bmatrix} , \tag{2}$$

the elastic coefficients $C^k_{rs}(z)$ are constant in the case of classical material layers.

The compact formulation of geometrical relations for spherical shells with constant radii of curvature is:

$$\boldsymbol{\epsilon}^k = \boldsymbol{\Delta}(z)\boldsymbol{u}^k \,, \tag{3}$$

where the displacement vector is $\boldsymbol{u}^k = \{u^k\, v^k\, w^k\}^T$. The 6×3 matrix $\boldsymbol{\Delta}(z)$ has the following components:

$$\boldsymbol{\Delta}(z) = \begin{bmatrix} \frac{1}{H_\alpha(z)}\frac{\partial}{\partial\alpha} & 0 & \frac{1}{H_\alpha(z)R_\alpha} \\ 0 & \frac{1}{H_\beta(z)}\frac{\partial}{\partial\beta} & \frac{1}{H_\beta(z)R_\beta} \\ 0 & 0 & \frac{\partial}{\partial z} \\ 0 & \frac{\partial}{\partial z} - \frac{1}{H_\beta(z)R_\beta} & \frac{1}{H_\beta(z)}\frac{\partial}{\partial\beta} \\ \frac{\partial}{\partial z} - \frac{1}{H_\alpha(z)R_\alpha} & 0 & \frac{1}{H_\alpha(z)}\frac{\partial}{\partial\alpha} \\ \frac{1}{H_\beta(z)}\frac{\partial}{\partial\beta} & \frac{1}{H_\alpha(z)}\frac{\partial}{\partial\alpha} & 0 \end{bmatrix} , \tag{4}$$

symbol ∂ is used for the partial derivatives performed with respect to the coordinate system (α, β, z). Radii of curvature are R_α and R_β, they are defined at the reference surface Ω_0 in the middle of the thickness. Parametric coefficients $H_\alpha(z)$ and $H_\beta(z)$ are defined as:

$$H_\alpha(z) = (1 + \frac{z}{R_\alpha}) = (1 + \frac{\tilde{z} - h/2}{R_\alpha}) \ , \quad H_\beta(z) = (1 + \frac{z}{R_\beta}) = (1 + \frac{\tilde{z} - h/2}{R_\beta}) \ , \quad H_z = 1 \ , \tag{5}$$

H_α and H_β can depend on z (that varies from $-h/2$ to $+h/2$ and it is referred to Ω_0 surface) or on $\tilde{z}$ coordinate (that varies from 0 to h and it is referred to the bottom surface) [44].

The developed three-dimensional shell theory employs the general three-dimensional differential equilibrium relations developed in the general orthogonal curvilinear system (α, β, z) for multilayered spherical panels. Mean radii of curvature R_α and R_β are constant because they are evaluated at the reference surface:

$$H_\beta(z)\frac{\partial \sigma^k_{\alpha\alpha}}{\partial \alpha} + H_\alpha(z)\frac{\partial \sigma^k_{\alpha\beta}}{\partial \beta} + H_\alpha(z)H_\beta(z)\frac{\partial \sigma^k_{\alpha z}}{\partial z} + (\frac{2H_\beta(z)}{R_\alpha} + \frac{H_\alpha(z)}{R_\beta})\sigma^k_{\alpha z} = 0 \ , \tag{6}$$

$$H_\beta(z)\frac{\partial \sigma^k_{\alpha\beta}}{\partial \alpha} + H_\alpha(z)\frac{\partial \sigma^k_{\beta\beta}}{\partial \beta} + H_\alpha(z)H_\beta(z)\frac{\partial \sigma^k_{\beta z}}{\partial z} + (\frac{2H_\alpha(z)}{R_\beta} + \frac{H_\beta(z)}{R_\alpha})\sigma^k_{\beta z} = 0 \ , \tag{7}$$

$$H_\beta(z)\frac{\partial \sigma^k_{\alpha z}}{\partial \alpha} + H_\alpha(z)\frac{\partial \sigma^k_{\beta z}}{\partial \beta} + H_\alpha(z)H_\beta(z)\frac{\partial \sigma^k_{zz}}{\partial z} - \frac{H_\beta(z)}{R_\alpha}\sigma^k_{\alpha\alpha} - \frac{H_\alpha(z)}{R_\beta}\sigma^k_{\beta\beta} + (\frac{H_\beta(z)}{R_\alpha} + \frac{H_\alpha(z)}{R_\beta})\sigma^k_{zz} = 0 \ , \tag{8}$$

the most general form of these equations for shells with variable radii of curvature are indicated in [45] and [46]. Eqs.(3)-(8) are defined for the spherical panel case and they easily degenerate in equations for cylindrical panels and for plates considering one or two radii of curvature as infinite (this feature gives one or two parametric coefficients equal 1). The employed index k in Eqs.(1)-(8) varies from 1 to N_L where N_L is the total number of physical layers. Constant elastic coefficients in Eqs.(1)-(2) and constant parametric coefficients through the thickness (see Eqs.(3)-(8)) are obtained if each physical k layer and the entire coordinate z are divided in an appropriate number of mathematical layers. As a consequence, the global number of mathematical and physical layers is M and the new index j varies from 1 to M. The new index j is employed in the above Eqs.(1)-(8) and in all the new equations that will be developed in the next part in order to obtain constant coefficients for shells and FGM layers.

The proposed general three-dimensional shell theory can be developed in closed form if simply supported sides and harmonic forms for displacements, loads and stresses are employed:

$$\{w^j, p^j_\alpha, \sigma^j_{\alpha z}\}(\alpha, \beta, z) = \{U^j, P^j_\alpha, \Sigma^j_{\alpha z}\}(z) cos(\bar{\alpha}\alpha) sin(\bar{\beta}\beta) \ , \tag{9}$$

$$\{v^j, p^j_\beta, \sigma^j_{\beta z}\}(\alpha, \beta, z) = \{V^j, P^j_\beta, \Sigma^j_{\beta z}\}(z) sin(\bar{\alpha}\alpha) cos(\bar{\beta}\beta) \ , \tag{10}$$

$$\{w^j, p^j_z, \sigma^j_{\alpha\alpha}, \sigma^j_{\beta\beta}, \sigma^j_{zz}\}(\alpha, \beta, z) = \{W^j, P^j_z, \Sigma^j_{\alpha\alpha}, \Sigma^j_{\beta\beta}, \Sigma^j_{zz}\}(z) sin(\bar{\alpha}\alpha) sin(\bar{\beta}\beta) \ , \tag{11}$$

$$\sigma^j_{\alpha\beta}(\alpha, \beta, z) = \Sigma^j_{\alpha\beta}(z) cos(\bar{\alpha}\alpha) cos(\bar{\beta}\beta) \ . \tag{12}$$

The index j is used for the indication of mathematical layers. The system (α, β, z) is constituted by general orthogonal curvilinear coordinates. U^j, V^j and W^j are the three displacement amplitudes in directions α, β and z, respectively. P^j_α, P^j_β and P^j_z are the three load amplitudes in directions α, β and z, respectively. $\Sigma^j_{\alpha\alpha}$, $\Sigma^j_{\beta\beta}$, Σ^j_{zz}, $\Sigma^j_{\beta z}$, $\Sigma^j_{\alpha z}$ and $\Sigma^j_{\alpha\beta}$ are the stress amplitudes. Terms $\bar{\alpha} = \frac{m\pi}{a}$ and $\bar{\beta} = \frac{n\pi}{b}$ are calculated using half-wave numbers m and n and the shell dimensions a and b in α and β directions. These last quantities are evaluated at the reference surface Ω_0 of the structure. The mid surface Ω_0 of a 3D shell is equidistant from the external surfaces. The distance between the external surfaces evaluated along the direction perpendicular to the mid-surface Ω_0 is the global thickness h of

the shell [47], [48]. Mean radii of curvature R_α and R_β are defined in α and β directions at the reference mid-surface Ω_0.

Proposed structures are simply supported along the edges:

$$w = v = 0,\ \sigma_{\alpha\alpha} = 0 \quad \text{for} \quad \alpha = 0, a\,, \tag{13}$$

$$w = u = 0,\ \sigma_{\beta\beta} = 0 \quad \text{for} \quad \beta = 0, b\,, \tag{14}$$

conditions given by Eqs.(13) and (14) are automatically satisfied thanks the harmonic forms written in Eqs.(9)-(12) for displacements and stresses. The load conditions at the external surfaces in the three directions z, α and β are imposed as:

$$\sigma_{zz} = p_z\,, \quad \sigma_{\alpha z} = p_\alpha\,, \quad \sigma_{\beta z} = p_\beta \quad \text{for} \quad z = -h/2, +h/2 \quad \text{or} \quad \tilde{z} = 0, h\,, \tag{15}$$

loads p_z, p_α and p_β are imposed as transverse normal and transverse shear stresses at the top and at the bottom of the entire multilayered plate or shell.

The substitution of Eqs.(1)-(4) and (9)-(12) in the 3D equilibrium Eqs.(6)-(8) gives the relative closed form:

$$\begin{aligned}
&\Big(- \frac{C^j_{55}H^j_\beta}{H^j_\alpha R^2_\alpha} - \frac{C^j_{55}}{R_\alpha R_\beta} - \bar\alpha^2\frac{C^j_{11}H^j_\beta}{H^j_\alpha} - \bar\beta^2\frac{C^j_{66}H^j_\alpha}{H^j_\beta}\Big)U^j + \Big(- \bar\alpha\bar\beta C^j_{12} - \bar\alpha\bar\beta C^j_{66}\Big)V^j + \\
&\Big(\bar\alpha\frac{C^j_{11}H^j_\beta}{H^j_\alpha R_\alpha} + \bar\alpha\frac{C^j_{12}}{R_\beta} + \bar\alpha\frac{C^j_{55}H^j_\beta}{H^j_\alpha R_\alpha} + \bar\alpha\frac{C^j_{55}}{R_\beta}\Big)W^j + \Big(\frac{C^j_{55}H^j_\beta}{R_\alpha} + \frac{C^j_{55}H^j_\alpha}{R_\beta}\Big)U^j_{,z} + \Big(\bar\alpha C^j_{13}H^j_\beta + \\
&\bar\alpha C^j_{55}H^j_\beta\Big)W^j_{,z} + \Big(C^j_{55}H^j_\alpha H^j_\beta\Big)U^j_{,zz} = 0\,,
\end{aligned} \tag{16}$$

$$\begin{aligned}
&\Big(- \bar\alpha\bar\beta C^j_{66} - \bar\alpha\bar\beta C^j_{12}\Big)U^j + \Big(- \frac{C^j_{44}H^j_\alpha}{H^j_\beta R^2_\beta} - \frac{C^j_{44}}{R_\alpha R_\beta} - \bar\alpha^2\frac{C^j_{66}H^j_\beta}{H^j_\alpha} - \bar\beta^2\frac{C^j_{22}H^j_\alpha}{H^j_\beta}\Big)V^j + \\
&\Big(\bar\beta\frac{C^j_{44}H^j_\alpha}{H^j_\beta R_\beta} + \bar\beta\frac{C^j_{44}}{R_\alpha} + \bar\beta\frac{C^j_{22}H^j_\alpha}{H^j_\beta R_\beta} + \bar\beta\frac{C^j_{12}}{R_\alpha}\Big)W^j + \Big(\frac{C^j_{44}H^j_\alpha}{R_\beta} + \frac{C^j_{44}H^j_\beta}{R_\alpha}\Big)V^j_{,z} + \Big(\bar\beta C^j_{44}H^j_\alpha + \\
&\bar\beta C^j_{23}H^j_\alpha\Big)W^j_{,z} + \Big(C^j_{44}H^j_\alpha H^j_\beta\Big)V^j_{,zz} = 0\,,
\end{aligned} \tag{17}$$

$$\begin{aligned}
&\Big(\bar\alpha\frac{C^j_{55}H^j_\beta}{H^j_\alpha R_\alpha} - \bar\alpha\frac{C^j_{13}}{R_\beta} + \bar\alpha\frac{C^j_{11}H^j_\beta}{H^j_\alpha R_\alpha} + \bar\alpha\frac{C^j_{12}}{R_\beta}\Big)U^j + \Big(\bar\beta\frac{C^j_{44}H^j_\alpha}{H^j_\beta R_\beta} - \bar\beta\frac{C^j_{23}}{R_\alpha} + \bar\beta\frac{C^j_{22}H^j_\alpha}{H^j_\beta R_\beta} + \bar\beta\frac{C^j_{12}}{R_\alpha}\Big)V^j + \\
&\Big(\frac{C^j_{13}}{R_\alpha R_\beta} + \frac{C^j_{23}}{R_\alpha R_\beta} - \frac{C^j_{11}H^j_\beta}{H^j_\alpha R^2_\alpha} - \frac{2C^j_{12}}{R_\alpha R_\beta} - \frac{C^j_{22}H^j_\alpha}{H^j_\beta R^2_\beta} - \bar\alpha^2\frac{C^j_{55}H^j_\beta}{H^j_\alpha} - \bar\beta^2\frac{C^j_{44}H^j_\alpha}{H^j_\beta}\Big)W^j + \\
&\Big(- \bar\alpha C^j_{55}H^j_\beta - \bar\alpha C^j_{13}H^j_\beta\Big)U^j_{,z} + \Big(- \bar\beta C^j_{44}H^j_\alpha - \bar\beta C^j_{23}H^j_\alpha\Big)V^j_{,z} + \Big(\frac{C^j_{33}H^j_\beta}{R_\alpha} + \frac{C^j_{33}H^j_\alpha}{R_\beta}\Big)W^j_{,z} + \\
&\Big(C^j_{33}H^j_\alpha H^j_\beta\Big)W^j_{,zz} = 0\,.
\end{aligned} \tag{18}$$

The above system composed by Eqs.(16)-(18) is a system of three second order partial differential equations in z. It gives a general three-dimensional shell model where the relations are written for spherical panels and they automatically degenerate in those for cylindrical shells and plates simply considering one radius of curvature or both radii of curvature as infinite. The compact system has already been presented in [29] and [30]. The coefficients are always constant, even if shell structures and FGM layers are investigated, because of the introduction of the j mathematical layers. The compact system of Eqs.(16)-(18) is reduced in a system of first order differential equations in z simply doubling

the number of variables as demonstrated in [32]- [35]. This final compact form for a j generical layer is:

$$\boldsymbol{D}^j \frac{\partial \boldsymbol{U}^j}{\partial \tilde{z}} = \boldsymbol{A}^j \boldsymbol{U}^j \ , \tag{19}$$

the meaning of vectors in Eq.(19) is $\frac{\partial \boldsymbol{U}^j}{\partial \tilde{z}} = \boldsymbol{U}^{j\prime}$ and $\boldsymbol{U}^j = [U^j \ V^j \ W^j \ U^{j\prime} \ V^{j\prime} \ W^{j\prime}]$. The employed thickness coordinate $\tilde{z}$ varies from 0 at the bottom to h at the top. The present work considers different load boundary conditions with respect to papers [29] and [30] in order to analyze new benchmarks subjected to different load combinations. The omitted steps are detailed in past author's works where the static analysis was performed when only a transverse normal load is applied [29], [30]. The compact system of Eq.(19) is solved using the exponential matrix method as proposed in [32]- [35]. System in Eq.(19) can be rearranged as:

$$\boldsymbol{D}^j \boldsymbol{U}^{j\prime} = \boldsymbol{A}^j \boldsymbol{U}^j \ , \tag{20}$$

$$\boldsymbol{U}^{j\prime} = \boldsymbol{D}^{j\,-1} \boldsymbol{A}^j \ \boldsymbol{U}^j \ , \tag{21}$$

$$\boldsymbol{U}^{j\prime} = \boldsymbol{A}^{j*} \ \boldsymbol{U}^j \ , \tag{22}$$

where $\boldsymbol{A}^{j*} = \boldsymbol{D}^{j\,-1} \boldsymbol{A}^j$. Coefficients in matrices $\boldsymbol{D}^j$, $\boldsymbol{A}^j$ and $\boldsymbol{A}^{j*}$ are not variable in z because of the introduction of j mathematical layers to consider the shell geometry and the functionally graded laws for the materials. Constant coefficients, thanks the index j, allow to write the solution of Eq.(22) as done in [33] and [34]:

$$\boldsymbol{U}^j(\tilde{z}^j) = exp(\boldsymbol{A}^{j*} \tilde{z}^j) \boldsymbol{U}^j(0) \quad \text{with} \quad \tilde{z}^j \ \epsilon \ [0, h^j] \ , \tag{23}$$

the coordinate $\tilde{z}^j$ is defined for each j layer (it varies from 0 at the bottom to h^j at the top). The exponential matrix is expanded by means of $\tilde{z}^j = h^j$ for each mathematical j layer:

$$\boldsymbol{A}^{j**} = exp(\boldsymbol{A}^{j*} h^j) = \boldsymbol{I} + \boldsymbol{A}^{j*} \, h^j + \frac{\boldsymbol{A}^{j*2}}{2!} {h^j}^2 + \frac{\boldsymbol{A}^{j*3}}{3!} {h^j}^3 + \ldots + \frac{\boldsymbol{A}^{j*N}}{N!} {h^j}^N \ , \tag{24}$$

the identity matrix $\boldsymbol{I}$ has dimension 6×6. The layer-wise method is based on the interlaminar continuity of displacements (compatibility conditions):

$$u_b^j = u_t^{j-1} \ , \ \ v_b^j = v_t^{j-1} \ , \ \ w_b^j = w_t^{j-1} \ , \tag{25}$$

and of transverse normal/shear stresses (equilibrium conditions):

$$\sigma_{zzb}^j = \sigma_{zzt}^{j-1} \ , \ \ \sigma_{\alpha zb}^j = \sigma_{\alpha zt}^{j-1} \ , \ \ \sigma_{\beta zb}^j = \sigma_{\beta zt}^{j-1} \ , \tag{26}$$

displacements and transverse stresses at the top (t) of the j-1 layer must be equal to relative displacements and transverse stresses at the bottom (b) of the j layer.

The introduction in the solution of the compatibility conditions proposed in Eq.(25), the equilibrium conditions proposed in Eq.(26) and the appropriate expansion for the exponential matrix shown in Eq.(24) gives the following final system:

$$\left[\begin{array}{c} \boldsymbol{B}^M(h^M) \ \boldsymbol{H}_m \\ \boldsymbol{B}^1(0) \end{array} \right] \ \boldsymbol{U}^1(0) \ = \ \boldsymbol{P} \ \ , \tag{27}$$

where the matrix $\boldsymbol{E}$ has dimension 6×6:

$$\boldsymbol{E} \ = \left[\begin{array}{c} \boldsymbol{B}^M(h^M) \ \boldsymbol{H}_m \\ \boldsymbol{B}^1(0) \end{array} \right] , \tag{28}$$

the vector $\boldsymbol{U}^1(0)$ of unknowns calculated at the bottom of the first layer and vector $\boldsymbol{P}$ of loads have dimension 6×1:

$$\boldsymbol{U}^1(0) \;=\; \begin{bmatrix} U^1(0) \\ V^1(0) \\ W^1(0) \\ U^{1\prime}(0) \\ V^{1\prime}(0) \\ W^{1\prime}(0) \end{bmatrix}, \qquad \boldsymbol{P} \;=\; \begin{bmatrix} P^M_{zt} \\ P^M_{\beta t} \\ P^M_{\alpha t} \\ P^1_{zb} \\ P^1_{\beta b} \\ P^1_{\alpha b} \end{bmatrix}. \tag{29}$$

M and 1 indicate last layer and first layer, respectively. Subscripts t and b indicate the top and the bottom of the specified layer, respectively. Matrices $\boldsymbol{B}^M(h^M)$ and $\boldsymbol{B}^1(0)$ include information about geometry and material properties of the proposed plate or shell considering the top of the last layer and the bottom of the first layer, respectively. Matrix $\boldsymbol{H}_m$ has been developed to consider the compatibility and equilibrium conditions at each mathematical and physical interface. From the Eq.(29), it is clear how considered loads can be applied at the top of the last layer M and at the bottom of the first layer 1 in z, β and α directions.

The following compact, linear and algebraic system must be solved:

$$\boldsymbol{E} \quad \boldsymbol{U}^1(0) \;=\; \boldsymbol{P} \;. \tag{30}$$

The vector $\boldsymbol{P}$ includes the possible load amplitudes considered at the external surfaces. The method is based on a layer-wise approach but the 6×6 matrix $\boldsymbol{E}$ has always the same dimension for any number M of employed mathematical layers and order of expansion N for the exponential matrix. This 3D exact shell solution has been implemented in the *3DES* code developed by the author in the Matlab environment as an in-house academic software. Spherical shell relations have been used in *3DES* code, and cylindrical shell and plate benchmarks are analyzed as particular cases. The vector $\boldsymbol{P}$ of loads in Eq.(29) can include several components depending on the boundary load conditions imposed in Eqs.(15). The possibilities to be analyzed can be σ_{zz} and/or $\sigma_{\alpha z}$ and/or $\sigma_{\beta z}$ equal 0 or equal the appropriate load amplitude considered at the top and/or at the bottom of the entire plate or shell. These possibilities allow several benchmarks as will be seen in Section 3 about results.

The vector $\boldsymbol{U}^1(0)$ containing the unknowns is obtained from the solution of the system indicated in Eq.(30). This vector includes the three displacements calculated at the bottom of the plate or shell and the relative derivatives peformed with respect to the z coordinate. From these six unknowns calculated at the bottom is possible to obtain the 6×1 vector $\boldsymbol{U}$ at each thickness position z using the compatibility and equilibrium conditions as shown in Eqs.(25) and (26). Strain and stress vectors are obtained at each thickness z coordinate using Eqs.(1)-(4). The proposed 3D shell method is very accurate in the calculation of displacements because of the layer-wise method. The strain vector is accurate because in Eqs.(3) and (4) the derivatives of displacements performed with respect to α and β coordinates are exactly calculated using the harmonic forms, and the derivatives of displacements performed with respect to z are directly calculated from the solution of the system indicated in Eq.(30). The proposed method has the same accuracy and potentiality of mixed methods because the derivatives of displacements made with respect to z have not been evaluated by means of any numerical procedure. As consequence, exact strain values in the z direction in Eqs.(3) and (4) allow correct stress values along z direction by using Eqs.(1) and (2).

3 Results

This section about results is organized in two main parts. The first part shows the validation of this 3D exact shell model by means of a literature overview where the proposed model has been compared with several 3D plate and shell models developed by other authors. The second part gives the new

benchmarks where for the first time the proposed general exact 3D shell model has been extended to the static analysis of functionally graded structures in the case of transverse normal and/or transverse shear loads simultaneously or separately applied at top and/or bottom external surfaces.

3.1 Validation of the model

The present general three-dimensional exact shell theory has been used for the free vibration investigation of single- and multi-layered plates and shells embedding isotropic, orthotropic, composite and functionally graded layers in [39]- [43] and for the free frequency investigation of single- and double-walled carbon nanotubes in [49] and [50], respectively. Then, the proposed 3D exact general model has been extended to the static analysis of plates and shells. 3D static analysis of one-layered and multilayered sandwich and composite structures subjected to transverse normal loads has been proposed in [29]. This type of analysis has been extended to functionally graded plates and shells in [30]. The extension to transverse shear and transverse normal loads applied to composite and sandwich plates and shells has been proposed in [31]. The present new work extends the static analysis in the case of several load combinations (see [31]) to functionally graded structures. The cases discussed in [39]- [43], [49]- [50] and [29]- [31] also proposed a lot of comparisons with different 3D analytical and numerical solutions presented in the literature. These assessments are sufficient to validate the model for the new benchmarks of the next section and to demonstrate how an order N=3 for the expansion of the exponential matrix and M=300 mathematical layers are always sufficient for the satisfactory analysis of all the cases proposed in the next part. In particular, a detailed convergence analysis was performed by the author in [42] for composite and sandwich plates and shells and in [43] for functionally graded plates and shells. This convergence investigation has been performed for different geometries, materials, thickness ratios and laminations sequences. From the results proposed in [42] and [43], it is clear how the order N=3 for the expansion of the exponential matrix and M=300 mathematical layers always guarantee the correct results. In details, in past author's works [39]- [43], [49] and [50] the present 3D shell model was successfully compared with the three-dimensional theories by Vel and Batra [7] and Srinivas et al. [51] for the free frequency analysis of isotropic square plates, with the 3D model by Armenakas et al. [52] for the vibration analysis of isotropic cylinders, with the 3D plate model by Messina [36] developed for mode analysis of composite laminated plates, with the 3D shell theory by Huang [53] for frequency analysis of laminated composite spherical and cylindrical shells, with the 3D plate model by Li et al. [9] for free vibrations of sandwich plates embedding an FGM core comprised between two external classical layers, with the 3D shell model by Zahedinejad et al. [12] for vibrations of cylindrical shell panels embedding a single FGM layer. Other validations were proposed in [29]- [31] for the static analysis of plates or shells subjected to transverse normal loads using the 3D plate solution by Pagano [54] for the bending of laminated composite and sandwich plates, the 3D method by Ren [55] for the static analysis of multilayered composite cylindrical shells, the 3D theory by Varadan and Bhaskar [56] for multilayered cylinders embedding composite layers, the 3D shell solution by Fan and Zhang [38] for multilayered spherical shells embedding composite layers, the 3D model by Kashtalyan [20] for single-layered FGM plates and the 3D model by Kashtalyan and Menshykova [21] for sandwich plates embedding a functionally graded material core. Table 1, extracted from the work [30], proposes the comparison between the present 3D shell model (when N=3 and M=300) and the 3D plate solution by Kashtalyan [20]. A square simply supported functionally graded plate is investigated when an harmonic transverse normal load is applied at the top surface (amplitude $P_z = 1Pa$ and half-wave numbers $m = n = 1$). The only FGM layer has a shear modulus changing through the thickness direction ($-h/2 \leq z \leq +h/2$) in accordance with the law $G(z) = G_0 e^{\gamma(z/h-0.5)}$. The isotropic material has Poisson ratio $\nu_0 = 0.3$. The in-plane dimensions are $a = b = 3m$ and the thickness value is $h = 1m$ (very thick plate). The no-dimensional transverse displacements $\bar{w} = -\frac{G_0 w}{P_z h}$ are evaluated at the middle of the plate when the parameter γ selected in the exponential law changes. The two 3D solutions are always coincident for

all γ parameters even if the plate is very thick.

The benchmarks proposed in this work analyze functionally graded plates and shells subjected to several combinations of transverse normal/shear loads at the external surfaces. This new formulation is obtained from past papers [29] and [30] about multilayered and FGM plates and shells simply modifying the load boundary conditions in order to change the load vector. These boundary load conditions in terms of stresses $\sigma_{\alpha z}$, $\sigma_{\beta z}$ and σ_{zz} are appropriately modified to consider the new load applications. However, the three-dimensional equilibrium relations and the solution procedure are the same seen for the models developed in [29] and [30] for transverse normal loads positioned at the top or at the bottom of the plates and shells. For these reasons, the use of values N=3 and M=300 is still here sufficient.

3.2 New benchmarks

The four new benchmarks are shown in Figures 1-4 where details about geometry, lamination, material law and applied loads are given. All the proposed structures are simply supported and the applied loads are in harmonic form.

Figure 1 proposes the first benchmark (B1) about the one-layered FGM square plate. The two plate dimensions are $a = b = 1m$ and thickness ratios a/h are 10 and 50. The Young modulus $E(z)$ in the FGM layer changes through the thickness direction as:

$$E(z) = E_m + (E_c - E_m)V_c\,, \tag{31}$$

where the Young modulus for the metallic phase is $E_m = 73GPa$, the Poisson ratio for the metallic phase is $\nu_m = 0.3$, the Young modulus of the ceramic phase is $E_c = 380GPa$ and the Poisson ratio of the ceramic phase is $\nu_c = 0.3$. The volume fraction V_c of the ceramic phase in Eq.(31) is:

$$V_c = \Big(\frac{2z+h}{2h}\Big)^p\,, \tag{32}$$

where $-h/2 \leq z \leq +h/2$ (h is the total thickness) and the exponential for the FGM law is $p = 0.5, 1.0, 2.0$. The transverse normal load has amplitude $P_z^t = -1Pa$ at the top and amplitude $P_z^b = +1Pa$ at the bottom considering half-wave numbers $m = n = 1$. Results for displacements and stresses are calculated in no-dimensional form:

$$\{\bar{u},\bar{v},\bar{w}\} = \frac{10^4 E_m\{u,v,w\}}{P_z^b h(a/h)^4}\,, \quad \{\bar{\sigma}_{\alpha\alpha},\bar{\sigma}_{\beta\beta},\bar{\sigma}_{\alpha\beta}\} = \frac{\{\sigma_{\alpha\alpha},\sigma_{\beta\beta},\sigma_{\alpha\beta}\}}{P_z^b(a/h)^2}\,, \tag{33}$$

$$\{\bar{\sigma}_{\alpha z},\bar{\sigma}_{\beta z}\} = \frac{10^2\{\sigma_{\alpha z},\sigma_{\beta z}\}}{P_z^b(a/h)}\,, \quad \bar{\sigma}_{zz} = \sigma_{zz}\,.$$

Figure 5 shows the three displacement amplitudes through the thickness direction when the thickness ratio is $a/h = 10$ and the exponent for the FGM law is $p = 0.5$. The plate is thick and functionally graded. For these reasons, constant displacements through the thickness are not possible. Compatibility conditions have been correctly imposed at each mathematical interface. Figure 6 proposes the six stress amplitudes through the thickness direction for the same thickness ratio and exponent p already considered for the displacement evaluation of Figure 5. The only functionally graded layer does not give any discontinuity in the evaluation of in-plane normal and in-plane shear stresses. Transverse shear and transverse normal stresses are continuous because only one FGM layer is embedded. Moreover, the equilibrium conditions have been correctly imposed in the proposed three-dimensional shell theory for each j mathematical layer. Transverse normal stress $\bar{\sigma}_{zz}$ at the top and at the bottom is equal to the applied transverse normal loads at the external surfaces ($P_z^t = -1Pa$ and $P_z^b = +1Pa$). Transverse shear stresses $\bar{\sigma}_{\alpha z}$ and $\bar{\sigma}_{\beta z}$ are zero at the external surfaces because no P_α and P_β loads have been applied at the top and/or bottom. The maximum values of transverse shear stresses through the

thickness direction are not at the middle surface because both high thickness values of the plate and functionally graded laws for the materials do not give any symmetry in z. Table 2 proposes the six stress amplitudes and the three displacement amplitudes at the top, middle and bottom of the plate for moderately thick ($a/h = 10$) and moderately thin ($a/h = 50$) plates when the exponential p for the FGM law is 0.5, 1.0 and 2.0. The same considerations discussed in Figures 5 and 6 are here extended to further thickness ratios and values of the exponent p. These quantitative values can be used to assess new numerical and analytical 3D or 2D models developed for functionally graded plates.

Figure 2 shows the second benchmark (B2) about the one-layered FGM cylinder. The structure has circumferential dimension $a = 2\pi R_\alpha$ and longitudinal dimension $b = 20m$, and radii of curvature $R_\alpha = 10m$ and $R_\beta = \infty$. The investigated thickness ratios R_α/h are 10 and 100. The Young modulus $E(z)$ in the FGM layer changes through the thickness direction with the same law already indicated in Eqs.(31) and (32). The data about the Young modulii, Poisson ratios, thickness coordinates and exponential for the FGM law do not change with respect to the benchmark 1 (B1). The applied transverse shear load has amplitude $P_\beta^t = +1Pa$ at the top and amplitude $P_\beta^b = -1Pa$ at the bottom using half-wave numbers $m = n = 2$. Results for displacements and stresses are calculated in no-dimensional form:

$$\{\bar{u}, \bar{v}, \bar{w}\} = \frac{10^4 E_m \{u, v, w\}}{P_\beta^t h (R_\alpha/h)^4}, \quad \{\bar{\sigma}_{\alpha\alpha}, \bar{\sigma}_{\beta\beta}, \bar{\sigma}_{\alpha\beta}\} = \frac{10^2 \{\sigma_{\alpha\alpha}, \sigma_{\beta\beta}, \sigma_{\alpha\beta}\}}{P_\beta^t (R_\alpha/h)^2}, \tag{34}$$

$$\{\bar{\sigma}_{\alpha z}, \bar{\sigma}_{zz}\} = \frac{10^2 \{\sigma_{\alpha z}, \sigma_{zz}\}}{P_\beta^t (R_\alpha/h)}, \quad \bar{\sigma}_{\beta z} = \sigma_{\beta z}\,.$$

Figure 7 proposes the three displacement amplitudes through the thickness direction when the thickness ratio is $R_\alpha/h = 10$ and the exponent for the FGM law is $p = 1.0$. The cylinder is thick and functionally graded. The variation of displacements through the thickness is evident and it is not linear because of the presence of the radius of curvature. Figure 8 gives the six stress amplitudes through the thickness direction for the same thickness ratio and exponent p considered for the displacement visualization. The only functionally graded layer does not give any discontinuity in the evaluation of in-plane normal and in-plane shear stresses. Transverse shear and transverse normal stresses are continuous because only one FGM layer is included. The equilibrium and compatibility conditions have been correctly imposed in the developed three-dimensional shell theory for all the mathematical interfaces. Transverse shear stress $\bar{\sigma}_{\beta z}$ at the top and at the bottom is equal to the positioned transverse shear loads at the external surfaces ($P_\beta^t = +1Pa$ and $P_\beta^b = -1Pa$). Transverse shear stress $\bar{\sigma}_{\alpha z}$ is zero at the external surfaces because no P_α loads are applied at the top and at the bottom. Transverse normal stress $\bar{\sigma}_{zz}$ is zero at the external surfaces because no P_z loads have been applied at the top and at the bottom. The maximum values of $\bar{\sigma}_{\alpha z}$ and $\bar{\sigma}_{zz}$ through the thickness direction are not at the middle surface because of the high thickness value of the cylinder. Moreover, the functionally graded law for the material does not give any symmetry in z. Table 3 proposes the six stress amplitudes and the three displacement amplitudes at the top, middle and bottom of the cylinder for moderately thick ($R_\alpha/h = 10$) and moderately thin ($R_\alpha/h = 100$) cylinders when the exponential p for the FGM law is 0.5, 1.0 and 2.0. The same considerations discussed in Figures 7 and 8 are here confirmed for additional thickness ratios and values of the exponent p. These quantitative values can be used to assess new numerical and analytical 3D or 2D models developed for functionally graded cylinders.

The third benchmark (B3) is summarized in Figure 3. It considers a sandwich cylindrical shell including a FGM core. The shell has dimensions $a = \frac{\pi}{3} R_\alpha$ and $b = 20m$, and radii of curvature $R_\alpha = 10m$ and $R_\beta = \infty$. The investigated thickness ratios R_α/h are 10 and 100. h is the global thickness. The bottom skin is completely metallic with Young modulus $E_m = 73GPa$, Poisson ratio $\nu_m = 0.3$ and thickness value $h_1 = 0.15h$. The top skin is completely ceramic with Young modulus $E_c = 200GPa$, Poisson ratio $\nu_c = 0.3$ and thickness value $h_3 = 0.15h$. The internal functionally graded

core has thickness $h_2 = 0.7h$ and the elastic properties vary with continuity from those of the bottom skin to those of the top skin using Eqs.(31) and (32) where $-0.7h/2 \leq z \leq +0.7h/2$ ($0.7h$ is the core thickness). The exponential for the FGM law is $p = 0.5, 1.0, 2.0$. In Eq.(32), the thickness h must be replaced by the thickness $0.7h$ of the core. The applied transverse shear load has amplitude $P_\beta^t = +1Pa$ at the top and amplitude $P_\beta^b = 0Pa$ at the bottom with half-wave numbers $m = n = 1$. Displacements and stresses have the same no-dimensional forms already seen in Eqs.(34) for the benchmark 2 (B2). Figure 9 proposes the three displacement amplitudes through the thickness direction when the thickness ratio is $R_\alpha/h = 10$ and the exponent for the FGM law is $p = 2.0$. The cylindrical shell is a sandwich configuration but the typical zigzag form of displacements is not clearly shown in the figure because the FGM core properties change with continuity from those of the full ceramic skin to those of the full metallic skin. Figure 10 shows the six stress components along the thickness direction for the same thickness ratio and exponent p considered for the displacement visualization of Figure 9. In-plane shear and in-plane normal stresses are continuous through the thickness direction even if a sandwich configuration is analyzed because of the use of the FGM core. However, the change in slope for skins and core is evident. Transverse shear and transverse normal stresses are continuous because of the use of the FGM core and because the equilibrium conditions for transverse stresses have been correctly introduced in the shell model. Transverse normal stress $\bar{\sigma}_{zz}$ at the top and at the bottom is equal zero because no external transverse normal loads P_z have been applied. Transverse shear stress $\bar{\sigma}_{\alpha z}$ is zero at the external surfaces because no transverse shear loads P_α have been applied at the top and at the bottom of the shell. Transverse shear stress $\bar{\sigma}_{\beta z}$ is zero at the bottom and equals one at the top because the load conditions are $P_\beta^b = 0Pa$ at the bottom and $P_\beta^t = +1Pa$ at the top, respectively. The maximum values of $\bar{\sigma}_{\alpha z}$ and $\bar{\sigma}_{zz}$ through the thickness direction is not at the middle surface because of the high thickness value of the cylindrical shell, the functionally graded law for the core and the different material for the two external skins. All these features do not give any symmetry in z. Table 4 proposes the three displacement components and the six stress components at the top, middle and bottom of the cylinder for moderately thick ($R_\alpha/h = 10$) and moderately thin ($R_\alpha/h = 100$) cylindrical shells when the exponential p for the FGM law is 0.5, 1.0 and 2.0. The same considerations discussed in Figures 9 and 10 are here confirmed for these additional thickness ratios and values of the exponent p. These quantitative values can be used to assess new numerical and analytical 3D or 2D models developed for sandwich cylindrical shells embedding an FGM core.

The last benchmark (B4) of Figure 4 considers a sandwich spherical shell embedding a FGM core. The dimensions of the structure are $a = b = \frac{\pi}{3}R_\alpha = \frac{\pi}{3}R_\beta$, where radii of curvature are $R_\alpha = R_\beta = 10m$ and thickness ratios R_α/h can be 10 or 100 (where h is the total thickness). The applied transverse shear load has amplitude $P_\alpha^t = +1Pa$ at the top and amplitude $P_\alpha^b = -1Pa$ at the bottom considering half-wave numbers $m = n = 1$. As clearly shown in Figures 3 and 4, cylindrical shell and spherical shell have the same lamination scheme and the same material properties. Therefore, the thickness of skins and core, elastic properties of skins and core and the FGM law do not change with respect to the benchmark 3 (B3). The no-dimensional forms of displacements and stresses are similar to those already proposed in Eqs.(34) for benchmarks 2 and 3. The only differences are the use of the load P_α^t in place of the load P_β^t, and the exchange of $\sigma_{\beta z}$ and $\bar{\sigma}_{\beta z}$ for $\sigma_{\alpha z}$ and $\bar{\sigma}_{\alpha z}$, respectively. Figure 11 proposes the three displacement amplitudes through the thickness direction when the thickness ratio is $R_\alpha/h = 10$ and the exponent for the FGM law is $p = 2.0$. The spherical shell is a sandwich configuration but the classical zigzag form of displacements is not shown because the core is in FGM. Compatibility conditions have been correctly imposed in the theory at each mathematical interface. Figure 12 gives the six stress amplitudes through the thickness direction for the same thickness ratio and exponent p already considered for the displacement visualization in Figure 11. In-plane shear and in-plane normal stresses are continuous through the thickness direction even if a sandwich configuration is analyzed because of the use of the FGM core. However, the change in slope for skins and core is clear. This feature is more evident with respect to the benchmark 3 about the cylindrical shell because

the presence of two radii of curvature in the spherical shell geometry gives a complete coupling between the three displacement components. Transverse shear and transverse normal stresses are continuous because of the use of the FGM core and because the equilibrium conditions for transverse stresses have been correctly introduced in the shell theory. Transverse normal stress $\bar{\sigma}_{zz}$ at the top and at the bottom is equal zero because no external transverse normal loads P_z have been applied. Transverse shear stress $\bar{\sigma}_{\beta z}$ is zero at the external surfaces because no transverse shear load P_β has been applied at the top and at the bottom of the shell. Transverse shear stress $\bar{\sigma}_{\alpha z}$ at the external surfaces is equal to the imposed values of transverse normal load P_α ($+1Pa$ at the top and $-1Pa$ at the bottom). The maximum values of $\bar{\sigma}_{\beta z}$ and $\bar{\sigma}_{zz}$ through the thickness direction is not at the middle surface because of the high thickness value of the spherical shell, the functionally graded law for the core and the different material for the two external skins. These features do not give any symmetry in z. Table 5 proposes the three displacement components and the six stress components at the top, middle and bottom of the spherical shell for moderately thick ($R_\alpha/h = 10$) and moderately thin ($R_\alpha/h = 100$) structures when the exponential p for the FGM law is 0.5, 1.0 and 2.0. The same considerations discussed in Figures 11 and 12 are here confirmed for these additional thickness ratios and values of the exponent p. These quantitative values can be used to assess new numerical and analytical 3D or 2D models developed for sandwich spherical shells embedding an FGM core.

4 Conclusions

The present paper proposes an exact general 3D shell model in layer-wise form for the static analysis of functionally graded structures. The investigated geometries are plates, cylinders, cylindrical shells and spherical shells. The first two geometries are considered as one-layered embedding a functionally graded material with different thickness laws. The last two geometries show a sandwich configuration where the FGM core is comprised between two classical external layers (complete ceramic at the top and complete metallic at the bottom). The novelty of the work, with respect the present state of the art, is the possibility of different load applications at the external surfaces of the considered structures. In particular, transverse shear and transverse normal loads can be simultaneously or separately applied at bottom and/or top external surfaces. The proposed general model gives correct 3D exact results for each geometry, thickness ratio, lamination scheme, functionally graded material and load combination. In each case the continuity of displacements and transverse stresses has been correctly introduced in the theory. Moreover, the external load boundary conditions are always satisfied. The advantages connected with the use of FGM layers or FGM cores in sandwich configurations have been further analyzed by demonstrating that the use of FGM cores allows the continuity of in-plane stresses at the interfaces between the core and the skins. This feature is not possible in classical sandwich configurations that do not make use of the FGM core. The advantage of the proposed 3D exact shell solution is the development of a unique tool for the layer wise analysis of different geometries (plates, cylinders, cylindrical and spherical panels) embedding isotropic, orthotropic, composite and functionally graded materials. Exact 3D solutions in the literature are usually less general than the model here proposed. A future development of the present work will be a possible extension to the finite element analysis in order to include boundary conditions different from the simply supported ones, loads different form the harmonic ones and lamination schemes different from the classical cross-ply configurations.

References

[1] M. Naebe and K. Shirvanimoghaddam, Functionally graded materials: a review of fabrication and properties, *Applied Materials Today*, 5, 223-245, 2016.

[2] S. Kumar, K.V.V.S. Murthy Reddy, A. Kumar and G. Rohini Devi, Development and characterization of polymer-ceramic continuous fiber reinforced functionally graded composites for aerospace application, *Aerospace Science and Technology*, 26, 185-191, 2013.

[3] P.L. Bishay, J. Sladek, V. Sladek and S.N. Atluri, Analysis of functionally graded magnetoelectroelastic composites using hybrid/mixed finite elements and node-wise material properties, *Computers, Materials & Continua*, 29, 213-262, 2012.

[4] G. Mattei, A. Tirella and A. Ahluwalia, Functionally Graded Materials (FGMs) with predictable and controlled gradient profiles: computational modelling and realisation, *CMES: Computer Modeling in Engineering & Sciences*, 87, 483-504, 2012.

[5] G. Giunta, S. Belouettar and A.J.M. Ferreira, A static analysis of three-dimensional functionally graded beams by hierarchical modelling and a collocation meshless solution method, *Acta Mechanica*, 227, 969-991, 2016.

[6] Sh. Hosseini-Hashemi, H. Salehipour and S.R. Atashipour, Exact three-dimensional free vibration analysis of thick homogeneous plates coated by a functionally graded layer, *Acta Mechanica*, 223, 2153-2166, 2012.

[7] S.S. Vel and R.C. Batra, Three-dimensional exact solution for the vibration of functionally graded rectangular plates, *Journal of Sound and Vibration*, 272, 703-730, 2004.

[8] C.Y. Dong, Three-dimensional free vibration analysis of functionally graded annular plates using the Chebyshev-Ritz method, *Materials and Design*, 42, 1518-1525, 2008.

[9] Q. Li, V.P. Iu and K.P. Kou, Three-dimensional vibration analysis of functionally graded material sandwich plates, *Journal of Sound and Vibration*, 311, 498-515, 2008.

[10] P. Malekzadeh, Three-dimensional free vibration analysis of thick functionally graded plates on elastic foundations, *Composite Structures*, 89, 367-373, 2009.

[11] A. Alibeigloo, A.M. Kani and M.H. Pashaei, Elasticity solution for the free vibration analysis of functionally graded cylindrical shell bonded to thin piezoelectric layers, *International Journal of Pressure Vessels and Piping*, 89, 98-111, 2012.

[12] P. Zahedinejad, P. Malekzadeh, M. Farid and G. Karami, A semi-analytical three-dimensional free vibration analysis of functionally graded curved panels, *International Journal of Pressure Vessels and Piping*, 87, 470-480, 2010.

[13] W.Q. Chen, Z.G. Bian and H.J. Ding, Three-dimensional vibration analysis of fluid-filled orthotropic FGM cylindrical shells, *International Journal of Mechanical Sciences*, 46, 159-171, 2004.

[14] S.S. Vel, Exact elasticity solution for the vibration of functionally graded anisotropic cylindrical shells, *Composite Structures*, 92, 2712-2727, 2010.

[15] J. Sladek, V. Sladek, J. Krivacek and C. Zhang, Meshless local Petrov-Galerkin method for stress and crack analysis in 3-D axisymmetric FGM bodies, *CMES: Computer Modeling in Engineering & Sciences*, 8, 259-270, 2005.

[16] J. Sladek, V. Sladek, C.L. Tan and S.N. Atluri, Analysis of transient heat conduction in 3D anisotropic functionally graded solids, by the MLPG method, *CMES: Computer Modeling in Engineering & Sciences*, 32, 161-174, 2008.

[17] J. Sladek, V. Sladek and P. Solek, Elastic analysis in 3D anisotropic functionally graded solids by the MLPG, *CMES: Computer Modeling in Engineering & Sciences*, 43, 223-252, 2009.

[18] Y. Xu and D. Zhou, Three-dimensional elasticity solution of functionally graded rectangular plates with variable thickness, *Composite Structures*, 91, 56-65, 2009.

[19] Z. Zhong and E.T. Shang, Three-dimensional exact analysis of a simply supported functionally gradient piezoelectric plate, *International Journal of Solids and Structures*, 40, 5335-5352, 2003.

[20] M. Kashtalyan, Three-dimensional elasticity solution for bending of functionally graded rectangular plates, *European Journal of Mechanics - A/Solids*, 23, 853-864, 2004.

[21] M. Kashtalyan and M. Menshykova, Three-dimensional elasticity solution for sandwich panels with a functionally graded core, *Composite Structures*, 87, 36-43, 2009.

[22] H. Norouzi and A. Alibeigloo, Three dimensional static analysis of viscoelastic FGM cylindrical panel using state space differential quadrature method, *European Journal of Mechanics - A/Solids*, 61, 254-266, 2017.

[23] B. Yang, S. Kitipornchai, Y.-F. Yang and J. Yang, 3D thermo-mechanical bending solution of functionally graded graphene reinforced circular and annular plates, *Applied Mathematical Modelling*, 49, 69-86, 2017.

[24] A. Alibeigloo, Three dimensional coupled thermoelasticity solution of sandwich plate with FGM core under thermal shock, *Composite Structures*, 177, 96-103, 2017.

[25] P. Kumari, A. Singh, R.K.N.D. Rajapakse and S. Kapuria, Three-dimensional static analysis of Levy-type functionally graded plate with in-plane stiffness variation, *Composite Structures*, 168, 780-791, 2017.

[26] G.G Sheng and X. Wang, Thermoelastic vibration and buckling analysis of functionally graded piezoelectric cylindrical shells, *Applied Mathematical Modelling*, 34, 2630-2643, 2010.

[27] G.G Sheng and X. Wang, Active control of functionally graded laminated cylindrical shells, *Composite Structures*, 90, 448-457, 2009.

[28] G.G Sheng and X. Wang, Studies on dynamic behavior of functionally graded cylindrical shells with PZT layers under moving loads, *Journal of Sound and Vibration*, 323, 772-789, 2009.

[29] S. Brischetto, Exact three-dimensional static analysis of single- and multi-layered plates and shells, *Composites. Part B, engineering*, 119, 230-252, 2017.

[30] S. Brischetto, A general exact elastic shell solution for bending analysis of functionally graded structures, *Composite Structures*, 175, 70-85, 2017.

[31] S. Brischetto, A closed-form 3D shell solution for multilayered structures subjected to different load combinations, *Aerospace Science and Technology*, 70, 29-46, 2017.

[32] Open document, *Systems of Differential Equations*, free available on http://www.math.utah.edu/gustafso/, accessed on 30th May 2013.

[33] W.E. Boyce and R.C. DiPrima, *Elementary Differential Equations and Boundary Value Problems*, John Wiley & Sons, Ltd., New York, 2001.

[34] D. Zwillinger, *Handbook of Differential Equations*, Academic Press, New York, 1997.

[35] C. Molery and C. Van Loan, Nineteen dubious ways to compute the exponential of a matrix, twenty-five years later, *SIAM Review*, 45, 1-46, 2003.

[36] A. Messina, Three dimensional free vibration analysis of cross-ply laminated plates through 2D and exact models, *3rd International Conference on Integrity, Reliability and Failure*, Porto (Portugal), 20-24 July 2009.

[37] K.P. Soldatos and J. Ye, Axisymmetric static and dynamic analysis of laminated hollow cylinders composed of monoclinic elastic layers, *Journal of Sound and Vibration*, 184, 245-259, 1995.

[38] J. Fan and J. Zhang, Analytical solutions for thick, doubly curved, laminated shells, *Journal of Engineering Mechanics*, 118, 1338-1356, 1992.

[39] S. Brischetto, Three-dimensional exact free vibration analysis of spherical, cylindrical, and flat one-layered panels, *Shock and Vibration*, vol.2014, 1-29, 2014.

[40] S. Brischetto, An exact 3D solution for free vibrations of multilayered cross-ply composite and sandwich plates and shells, *International Journal of Applied Mechanics*, 6, 1-42, 2014.

[41] S. Brischetto, Exact elasticity solution for natural frequencies of functionally graded simply-supported structures, *Computer Modeling in Engineering and Sciences*, 95, 391-430, 2013.

[42] S. Brischetto, Convergence analysis of the exponential matrix method for the solution of 3D equilibrium equations for free vibration analysis of plates and shells, *Composites. Part B, engineering*, 98, 453-471, 2016.

[43] S. Brischetto, Exponential matrix method for the solution of exact 3D equilibrium equations for free vibrations of functionally graded plates and shells, *Journal of Sandwich Structures and Materials*, online, https://doi.org/10.1177/1099636216686127, 2017.

[44] W. Soedel, *Vibration of Shells and Plates*, Marcel Dekker, Inc., New York, 2004.

[45] F.B. Hildebrand, E. Reissner and G.B. Thomas, *Notes on the Foundations of the Theory of Small Displacements of Orthotropic Shells*, NACA Technical Note No. 1833, Washington, 1949.

[46] F. Tornabene, *Meccanica delle Strutture a Guscio in Materiale Composito*, Societá Editrice Esculapio, Bologna (Italy), 2012.

[47] A.W. Leissa, *Vibration of Plates*, NASA SP-160, Washington, 1969.

[48] A.W. Leissa, *Vibration of Shells*, NASA SP-288, Washington, 1973.

[49] S. Brischetto, A continuum elastic three-dimensional model for natural frequencies of single-walled carbon nanotubes, *Composites. Part B, engineering*, 61, 222-228, 2014.

[50] S. Brischetto, A continuum shell model including van derWaals interaction for free vibrations of double-walled carbon nanotubes, *Computer Modeling in Engineering & Sciences*, 104, 305-327, 2015.

[51] S. Srinivas, A.K. Rao and C.V.J. Rao, Flexure of simply supported thick homogeneous and laminated rectangular plates, *Zeitschrift für Angewandte Mathematik und Mechanik*, 49, 449-458, 1969.

[52] A.E. Armenakas, D.C. Gazis and G. Herrmann, *Free Vibrations of Circular Cylindrical Shells*, Pergamon Press, Oxford, 1969.

[53] N.N. Huang, Exact analysis for three-dimensional free vibrations of cross-ply cylindrical and doubly-curved laminates, *Acta Mechanica*, 108, 23-34, 1995.

[54] N.J. Pagano, Exact solutions for rectangular bidirectional composites and sandwich plates, *Journal of Composite Materials*, 4, 20-34, 1970.

[55] J.G. Ren, Exact solutions for laminated cylindrical shells in cylindrical bending, *Composite Science and Technology*, 29, 169-187, 1987.

[56] T.K. Varadan and K. Bhaskar, Bending of laminated orthotropic cylindrical shells - an elasticity approach, *Composite Structures*, 17, 141-156, 1991.

γ	3D [20]	Present 3D
10^{-1}	-1.4146	-1.4146
10^{-2}	-1.3496	-1.3496
10^{-3}	-1.3433	-1.3433
10^{-4}	-1.3426	-1.3426
10^{-5}	-1.3426	-1.3426
10^{-6}	-1.3426	-1.3426
-10^{-1}	-1.2740	-1.2740
-10^{-2}	-1.3355	-1.3355
-10^{-3}	-1.3419	-1.3418
-10^{-4}	-1.3425	-1.3425
-10^{-5}	-1.3425	-1.3425
-10^{-6}	-1.3425	-1.3425

Table 1: Preliminary assessment, one-layered FGM plate. No-dimensional transverse displacement $\bar{w} = -\frac{G_0 w}{P_z h}$ calculated at $z = 0$. Present 3D solution (with N=3 and M=300) compared with the 3D solution proposed by Kashtalyan [20].

(α,β)	$\bar{u}$ $(0, \frac{b}{2})$	$\bar{v}$ $(\frac{a}{2}, 0)$	$\bar{w}$ $(\frac{a}{2}, \frac{b}{2})$	$\bar{\sigma}_{\alpha\alpha}$ $(\frac{a}{2}, \frac{b}{2})$	$\bar{\sigma}_{\beta\beta}$ $(\frac{a}{2}, \frac{b}{2})$	$\bar{\sigma}_{\alpha\beta}$ $(0, 0)$	$\bar{\sigma}_{zz}$ $(\frac{a}{2}, \frac{b}{2})$	$\bar{\sigma}_{\alpha z}$ $(0, \frac{b}{2})$	$\bar{\sigma}_{\beta z}$ $(\frac{a}{2}, 0)$
					$p = 0.5$				
					a/h=10				
$z = -h/2$	-29.616	-29.616	-169.96	0.1600	0.1600	-0.0839	1.0000	0.0000	0.0000
$z = 0$	-3.7973	-3.7973	-172.10	0.0682	0.0682	-0.0364	0.1368	-48.643	-48.643
$z = h/2$	22.136	22.136	-170.92	-0.5211	-0.5211	0.2783	-1.0000	0.0000	0.0000
					a/h=50				
$z = -h/2$	-5.9491	-5.9491	-165.26	0.1566	0.1566	-0.0842	1.0000	0.0000	0.0000
$z = 0$	-0.7642	-0.7642	-165.35	0.0681	0.0681	-0.0366	0.1367	-48.725	-48.725
$z = h/2$	4.4216	4.4216	-165.30	-0.5163	-0.5163	0.2779	-1.0000	0.0000	0.0000
					$p = 1.0$				
					a/h=10				
$z = -h/2$	-40.756	-40.756	-218.86	0.1885	0.1885	-0.0992	1.0000	0.0000	0.0000
$z = 0$	-7.5347	-7.5347	-221.94	0.1055	0.1055	-0.0564	0.2006	-47.657	-47.657
$z = h/2$	26.012	26.012	-220.75	-0.6112	-0.6112	0.3268	-1.0000	0.0000	0.0000
					a/h=50				
$z = -h/2$	-8.2125	-8.2125	-213.52	0.1857	0.1857	-0.0999	1.0000	0.0000	0.0000
$z = 0$	-1.5136	-1.5136	-213.66	0.1052	0.1052	-0.0566	0.2001	-47.743	-47.743
$z = h/2$	5.1881	5.1881	-213.61	-0.6054	-0.6054	0.3259	-1.0000	0.0000	0.0000
					$p = 2.0$				
					a/h=10				
$z = -h/2$	-54.404	-54.404	-278.87	0.2484	0.2484	-0.1315	1.0000	0.0000	0.0000
$z = 0$	-12.432	-12.432	-283.12	0.1150	0.1150	-0.0614	0.2191	-45.215	-45.215
$z = h/2$	30.341	30.341	-281.99	-0.7112	-0.7112	0.3807	-1.0000	0.0000	0.0000
					a/h=50				
$z = -h/2$	-10.992	-10.992	-271.28	0.2468	0.2468	-0.1328	1.0000	0.0000	0.0000
$z = 0$	-2.4844	-2.4844	-271.46	0.1140	0.1140	-0.0614	0.2171	-45.315	-45.315
$z = h/2$	6.0302	6.0302	-271.41	-0.7027	-0.7027	0.3783	-1.0000	0.0000	0.0000

Table 2: Benchmark 1, 3D exact displacements and stresses for the one-layered FGM square plate.

(α,β)	$\bar{u}$ $(0,\frac{b}{2})$	$\bar{v}$ $(\frac{a}{2},0)$	$\bar{w}$ $(\frac{a}{2},\frac{b}{2})$	$\bar{\sigma}_{\alpha\alpha}$ $(\frac{a}{2},\frac{b}{2})$	$\bar{\sigma}_{\beta\beta}$ $(\frac{a}{2},\frac{b}{2})$	$\bar{\sigma}_{\alpha\beta}$ $(0,0)$	$\bar{\sigma}_{zz}$ $(\frac{a}{2},\frac{b}{2})$	$\bar{\sigma}_{\alpha z}$ $(0,\frac{b}{2})$	$\bar{\sigma}_{\beta z}$ $(\frac{a}{2},0)$
					$p=0.5$				
					R_α/h=10				
$z=-h/2$	-1.2297	6.2824	3.7386	-0.0890	-2.3392	0.1239	0.0000	0.0000	-1.0000
$z=0$	-1.4920	5.3603	4.0047	0.1548	-6.6643	0.1027	-0.9147	0.2668	-0.1169
$z=h/2$	-1.7666	4.8295	4.2211	0.6579	-7.6952	-0.1902	0.0000	0.0000	1.0000
					R_α/h=100				
$z=-h/2$	-0.0164	0.0540	0.0344	0.0196×10^{-2}	-0.1986	0.1281×10^{-2}	0.0000	0.0000	-1.0000
$z=0$	-0.0166	0.0534	0.0346	0.4092×10^{-2}	-0.6644	0.1819×10^{-2}	-0.9265×10^{-2}	0.2426×10^{-2}	-0.2072
$z=h/2$	-0.0169	0.0528	0.0349	0.9716×10^{-2}	-0.8607	-0.0829×10^{-2}	0.0000	0.0000	1.0000
					$p=1.0$				
					R_α/h=10				
$z=-h/2$	-1.2567	8.0859	5.4533	-0.0617	-2.5766	0.1767	0.0000	0.0000	-1.0000
$z=0$	-1.6095	6.6903	5.7796	0.3276	-6.4372	0.1945	-0.9576	0.2817	-0.2285
$z=h/2$	-1.9779	5.8590	6.0329	1.2039	-9.2074	-0.1268	0.0000	0.0000	1.0000
					R_α/h=100				
$z=-h/2$	-0.0198	0.0663	0.0431	0.0894×10^{-2}	-0.2093	0.1682×10^{-2}	0.0000	0.0000	-1.0000
$z=0$	-0.0201	0.0655	0.0434	0.6111×10^{-2}	-0.6355	0.1715×10^{-2}	-0.9720×10^{-2}	1.2293×10^{-2}	-0.3303
$z=h/2$	-0.0204	0.0648	0.0437	1.5699×10^{-2}	-1.0543	0.0559×10^{-2}	0.0000	0.0000	1.0000
					$p=2.0$				
					R_α/h=10				
$z=-h/2$	-1.3605	11.811	7.9478	-0.0430	-3.4093	0.2733	0.0000	0.0000	-1.0000
$z=0$	-1.8461	8.7936	8.3712	0.3918	-5.5594	0.2354	-0.9722	0.2999	-0.3168
$z=h/2$	-2.3540	7.5206	8.6868	1.9551	-11.679	-0.0465	0.0000	0.0000	1.0000
					R_α/h=100				
$z=-h/2$	-0.0253	0.0857	0.0567	0.1888×10^{-2}	-0.2687	0.2515×10^{-2}	0.0000	0.0000	-1.0000
$z=0$	-0.0257	0.0847	0.0571	0.6772×10^{-2}	-0.5422	0.3017×10^{-2}	-0.9929×10^{-2}	0.2247×10^{-2}	-0.4291
$z=h/2$	-0.0262	0.0838	0.0575	2.4346×10^{-2}	-1.3601	0.2430×10^{-2}	0.0000	0.0000	1.0000

Table 3: Benchmark 2, 3D exact displacements and stresses for the one-layered FGM cylinder.

(α,β)	$\bar{u}$ $(0,\frac{b}{2})$	$\bar{v}$ $(\frac{a}{2},0)$	$\bar{w}$ $(\frac{a}{2},\frac{b}{2})$	$\bar{\sigma}_{\alpha\alpha}$ $(\frac{a}{2},\frac{b}{2})$	$\bar{\sigma}_{\beta\beta}$ $(\frac{a}{2},\frac{b}{2})$	$\bar{\sigma}_{\alpha\beta}$ $(0,0)$	$\bar{\sigma}_{zz}$ $(\frac{a}{2},\frac{b}{2})$	$\bar{\sigma}_{\alpha z}$ $(0,\frac{b}{2})$	$\bar{\sigma}_{\beta z}$ $(\frac{a}{2},0)$
					$p=0.5$				
					R_α/h=10				
$z=-h/2$	-34.275	10.357	-64.686	3.8755	-0.4643	-0.8128	0.0000	0.0000	0.0000
$z=0$	-26.060	15.457	-64.802	1.5422	-4.9097	0.4655	1.1740	-4.8336	0.1288
$z=h/2$	-17.865	20.770	-64.212	-5.9907	-10.736	3.2962	0.0000	0.0000	1.0000
					R_α/h=100				
$z=-h/2$	-0.4077	0.1913	-1.0812	0.0577	-0.2832	-0.0244	0.0000	0.0000	0.0000
$z=0$	-0.3935	0.1998	-1.0808	0.0135	-0.6950	-0.0159	0.0222	-0.0829	0.3361
$z=h/2$	-0.3792	0.2083	-1.0803	-0.1235	-0.9337	0.0276	0.0000	0.0000	1.0000
					$p=1.0$				
					R_α/h=10				
$z=-h/2$	-37.066	11.294	-69.277	4.2642	-0.4948	-0.8676	0.0000	0.0000	0.0000
$z=0$	-28.319	16.753	-69.417	1.6151	-4.3917	0.4145	1.1142	-4.6519	0.1064
$z=h/2$	-19.560	22.423	-68.805	-6.0842	-11.475	3.5133	0.0000	0.0000	1.0000
					R_α/h=100				
$z=-h/2$	-0.4511	0.2114	-1.1946	0.0658	-0.3124	-0.0273	0.0000	0.0000	0.0000
$z=0$	-0.4354	0.2208	-1.1942	0.0162	-0.6423	-0.0153	0.0222	-0.0825	0.3052
$z=h/2$	-0.4196	0.2302	-1.1936	-0.1310	-1.0302	0.0296	0.0000	0.0000	1.0000
					$p=2.0$				
					R_α/h=10				
$z=-h/2$	-39.884	12.515	-73.908	4.6435	-0.5728	-0.8896	0.0000	0.0000	0.0000
$z=0$	-30.617	18.342	-74.062	1.4841	-3.6450	0.3816	1.0759	-4.5411	0.0929
$z=h/2$	-21.309	24.376	-73.419	-6.1798	-12.344	3.8117	0.0000	0.0000	1.0000
					R_α/h=100				
$z=-h/2$	-0.5050	0.2366	-1.3358	0.0752	-0.3490	-0.0307	0.0000	0.0000	0.0000
$z=0$	-0.4874	0.2471	-1.3354	0.0163	-0.5503	-0.0134	0.0230	-0.0848	0.2855
$z=h/2$	-0.4698	0.2576	-1.3347	-0.1419	-1.1511	0.0326	0.0000	0.0000	1.0000

Table 4: Benchmark 3, 3D exact displacements and stresses for the sandwich cylindrical shell embedding a FGM core.

(α,β)	$\bar{u}$ $(0,\frac{b}{2})$	$\bar{v}$ $(\frac{a}{2},0)$	$\bar{w}$ $(\frac{a}{2},\frac{b}{2})$	$\bar{\sigma}_{\alpha\alpha}$ $(\frac{a}{2},\frac{b}{2})$	$\bar{\sigma}_{\beta\beta}$ $(\frac{a}{2},\frac{b}{2})$	$\bar{\sigma}_{\alpha\beta}$ $(0,0)$	$\bar{\sigma}_{zz}$ $(\frac{a}{2},\frac{b}{2})$	$\bar{\sigma}_{\alpha z}$ $(0,\frac{b}{2})$	$\bar{\sigma}_{\beta z}$ $(\frac{a}{2},0)$
				$p=0.5$					
				R_α/h=10					
$z=-h/2$	16.139	2.5003	18.052	-3.1462	0.1668	2.2638	0.0000	-1.0000	0.0000
$z=0$	13.575	-0.1403	18.279	-4.1926	2.8566	3.4524	-1.6845	0.0893	2.2257
$z=h/2$	11.809	-2.8019	18.202	-2.6501	6.1476	2.7117	0.0000	1.0000	0.0000
				R_α/h=100					
$z=-h/2$	0.1426	0.4049×10^{-2}	0.2106	-0.1739	0.1473	0.1700	0.0000	-1.0000	0.0000
$z=0$	0.1400	0.0894×10^{-2}	0.2107	-0.3600	0.3552	0.3622	-0.0193	-0.2034	0.0266
$z=h/2$	0.1376	-0.2260×10^{-2}	0.2107	-0.4101	0.4697	0.4257	0.0000	1.0000	0.0000
				$p=1.0$					
				R_α/h=10					
$z=-h/2$	18.049	2.9605	20.282	-3.5217	0.1436	2.5518	0.0000	-1.0000	0.0000
$z=0$	15.175	0.0181	20.541	-3.9339	2.5921	3.2708	-1.6686	0.0321	2.2574
$z=h/2$	13.137	-2.9634	20.460	-2.9090	6.7855	3.0629	0.0000	1.0000	0.0000
				R_α/h=100					
$z=-h/2$	0.1582	0.4720×10^{-2}	0.2340	-0.1930	0.1630	0.1890	0.0000	-1.0000	0.0000
$z=0$	0.1554	0.1218×10^{-2}	0.2340	-0.3345	0.3294	0.3372	-0.0193	-0.2651	0.0266
$z=h/2$	0.1527	-0.2285×10^{-2}	0.2340	-0.4549	0.5201	0.4731	0.0000	1.0000	0.0000
				$p=2.0$					
				R_α/h=10					
$z=-h/2$	20.276	3.4064	22.819	-3.9597	0.1383	2.8765	0.0000	-1.0000	0.0000
$z=0$	17.092	0.1239	23.113	-3.4261	2.1765	2.8422	-1.6514	0.0021	2.3270
$z=h/2$	14.755	-3.2169	23.028	-3.2787	7.5430	3.4739	0.0000	1.0000	0.0000
				R_α/h=100					
$z=-h/2$	0.1776	0.5478×10^{-2}	0.2628	-0.2166	0.1827	0.2123	0.0000	-1.0000	0.0000
$z=0$	0.1745	0.1545×10^{-2}	0.2629	-0.2880	0.2830	0.2906	-0.0195	-0.3012	0.0275
$z=h/2$	0.1714	-0.2389×10^{-2}	0.2628	-0.5105	0.5829	0.5317	0.0000	1.0000	0.0000

Table 5: Benchmark 4, 3D exact displacements and stresses for the sandwich spherical shell embedding a FGM core.

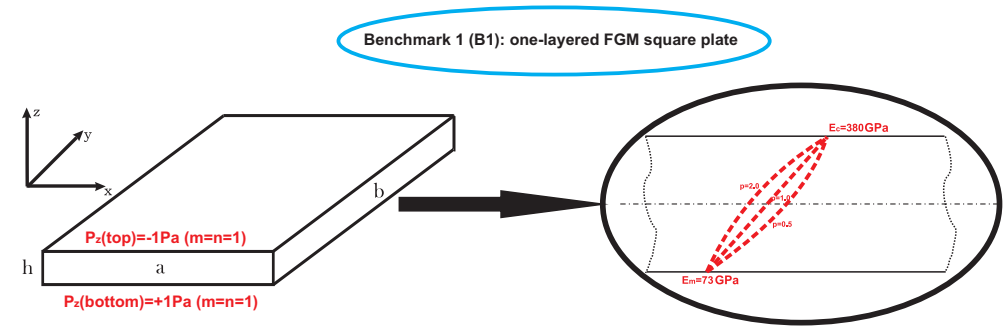

Figure 1: Geometry, lamination, materials and loads for the benchmark 1 (B1) about the one-layered FGM square plate.

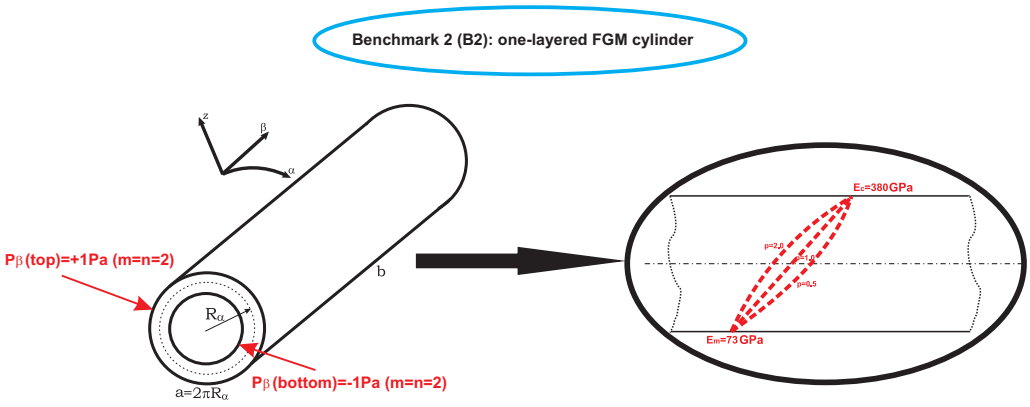

Figure 2: Geometry, lamination, materials and loads for the benchmark 2 (B2) about the one-layered FGM cylinder.

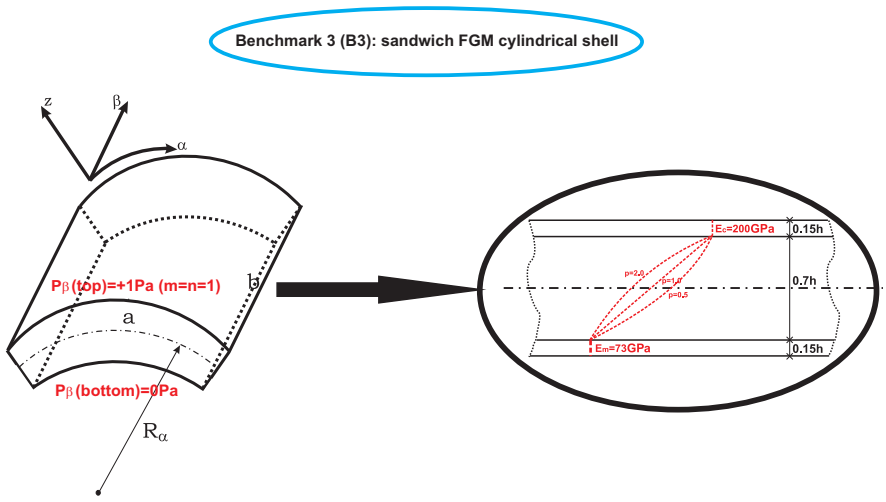

Figure 3: Geometry, lamination, materials and loads for the benchmark 3 (B3) about the sandwich cylindrical shell embedding a FGM core.

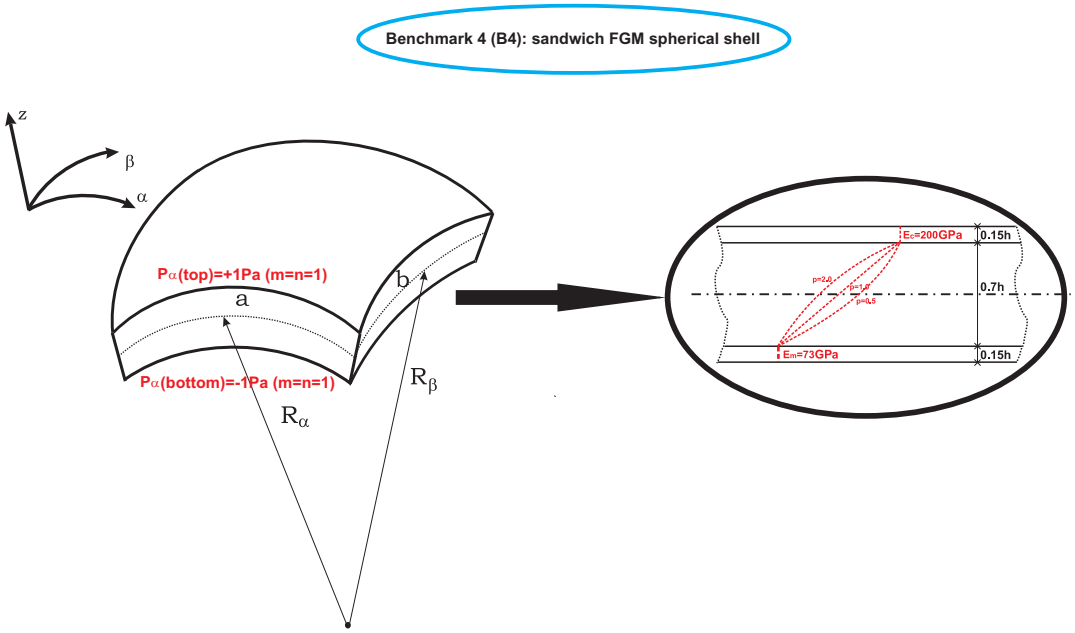

Figure 4: Geometry, lamination, materials and loads for the benchmark 4 (B4) about the sandwich spherical shell embedding a FGM core.

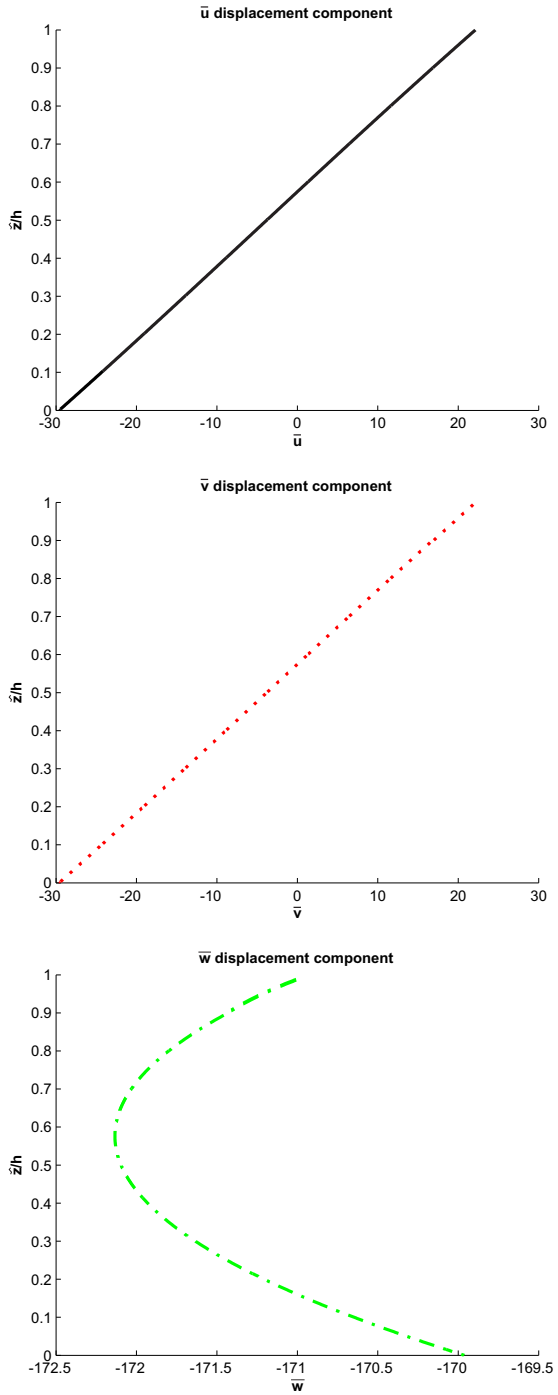

Figure 5: Benchmark 1, no-dimensional displacements through the thickness $\tilde{z}$ for $a/h = 10$ and $p = 0.5$.

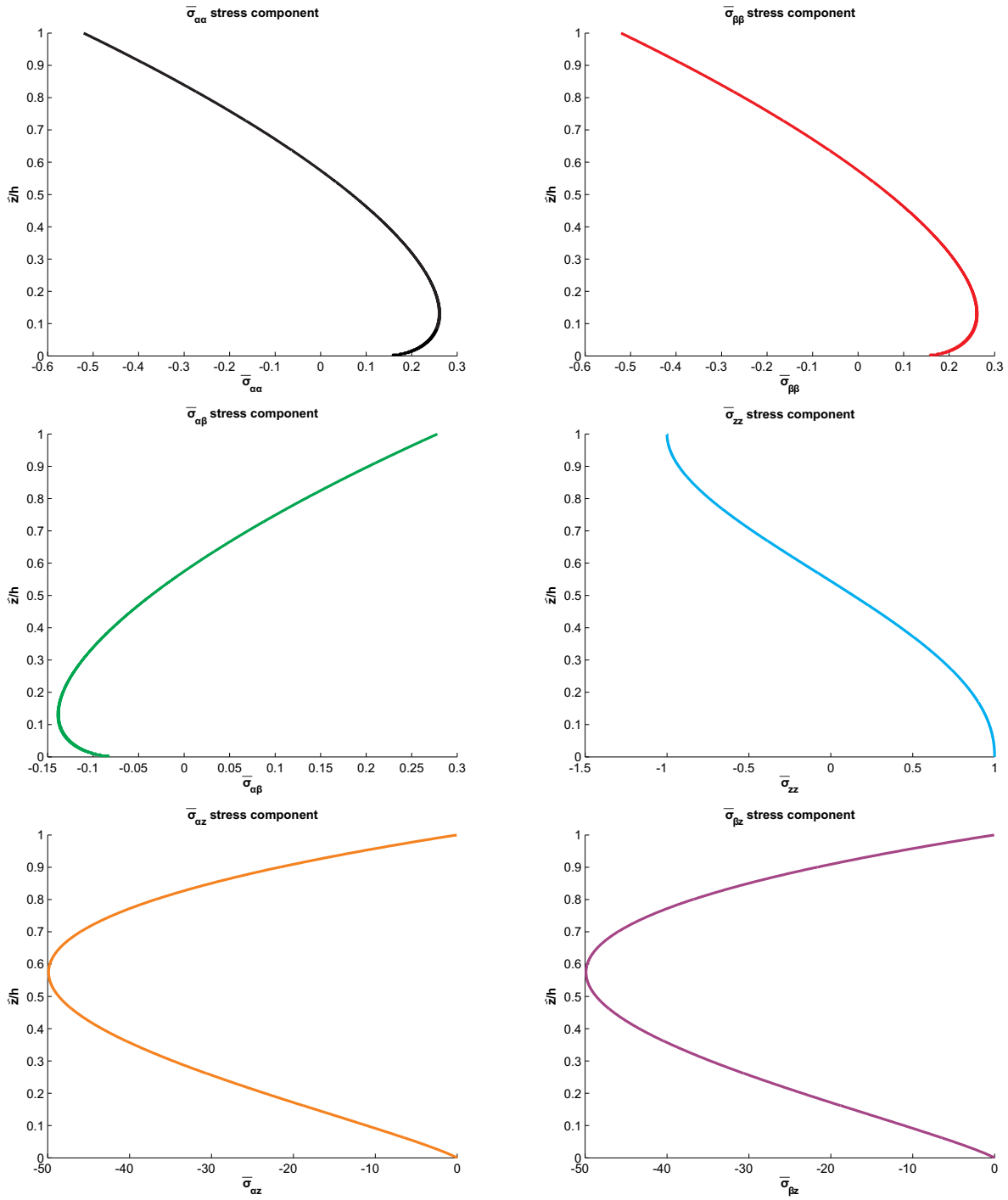

Figure 6: Benchmark 1, no-dimensional stresses through the thickness $\tilde{z}$ for $a/h = 10$ and $p = 0.5$.

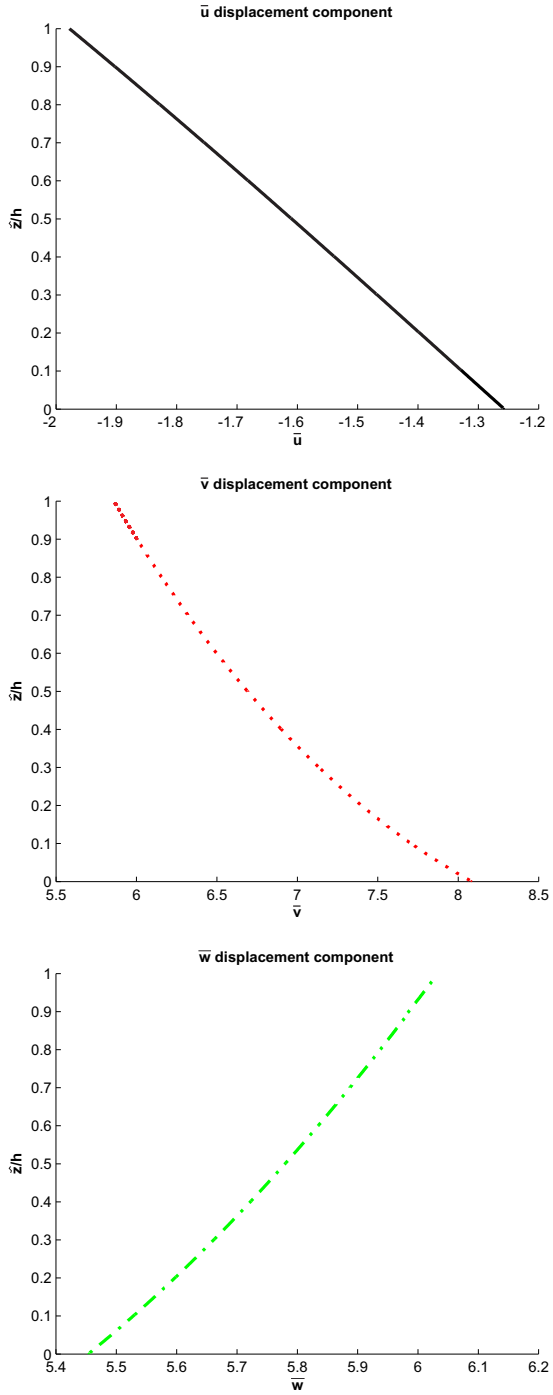

Figure 7: Benchmark 2, no-dimensional displacements through the thickness $\tilde{z}$ for $R_\alpha/h = 10$ and $p = 1.0$.

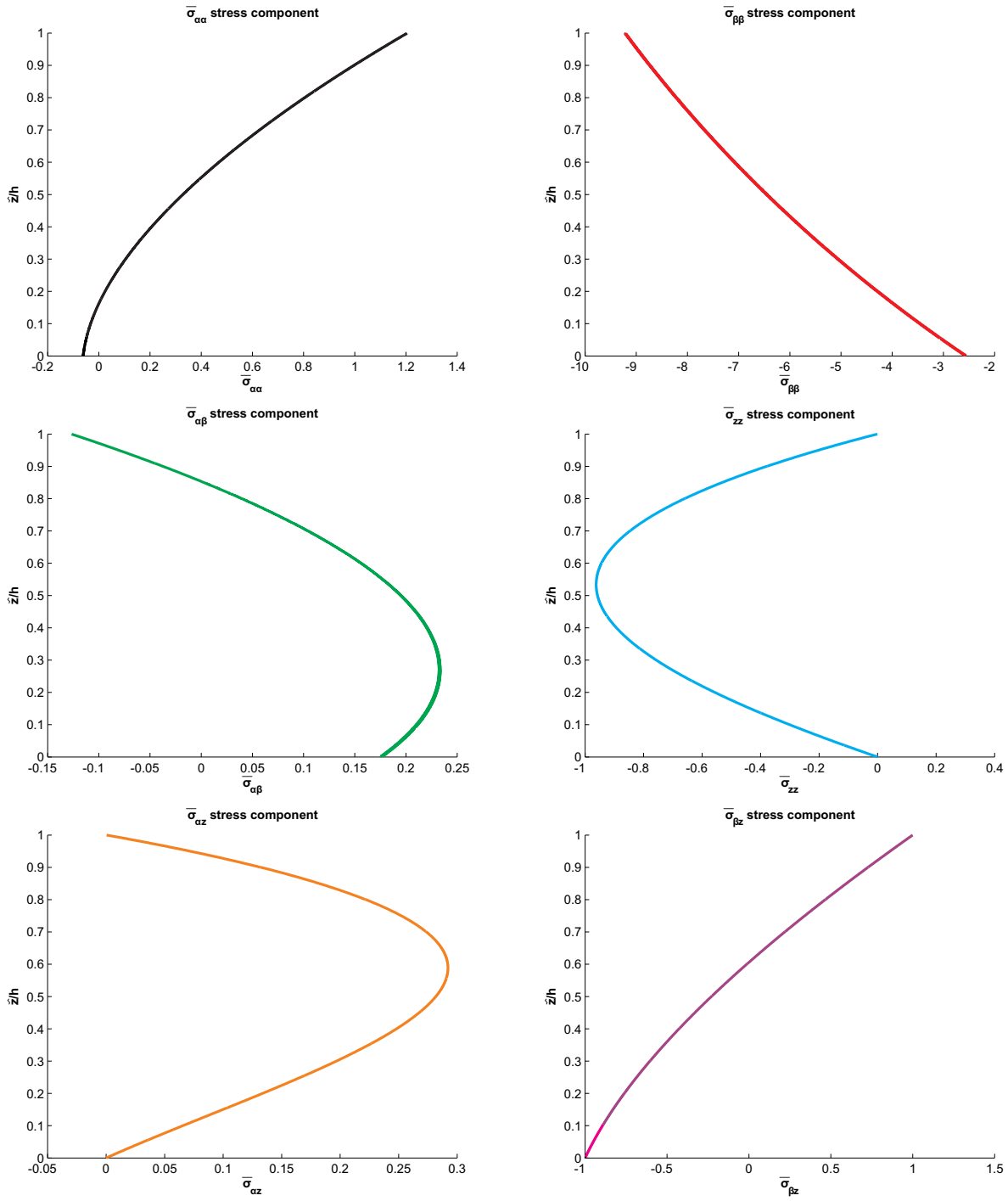

Figure 8: Benchmark 2, no-dimensional stresses through the thickness $\tilde{z}$ for $R_\alpha/h = 10$ and $p = 1.0$.

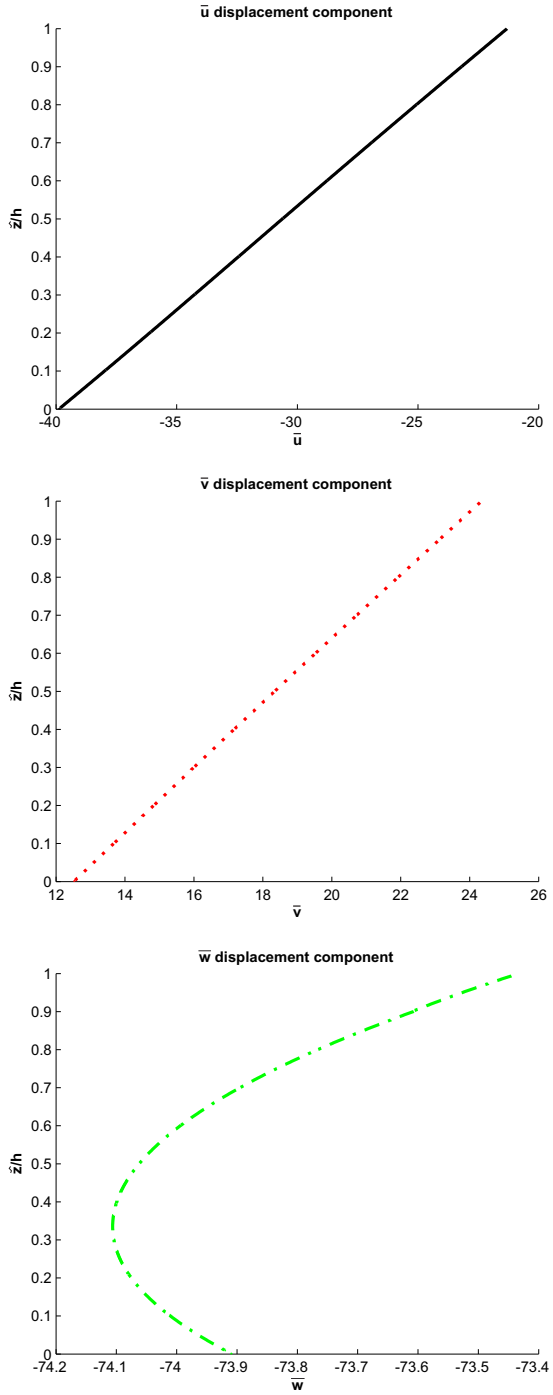

Figure 9: Benchmark 3, no-dimensional displacements through the thickness $\tilde{z}$ for $R_\alpha/h = 10$ and $p = 2.0$.

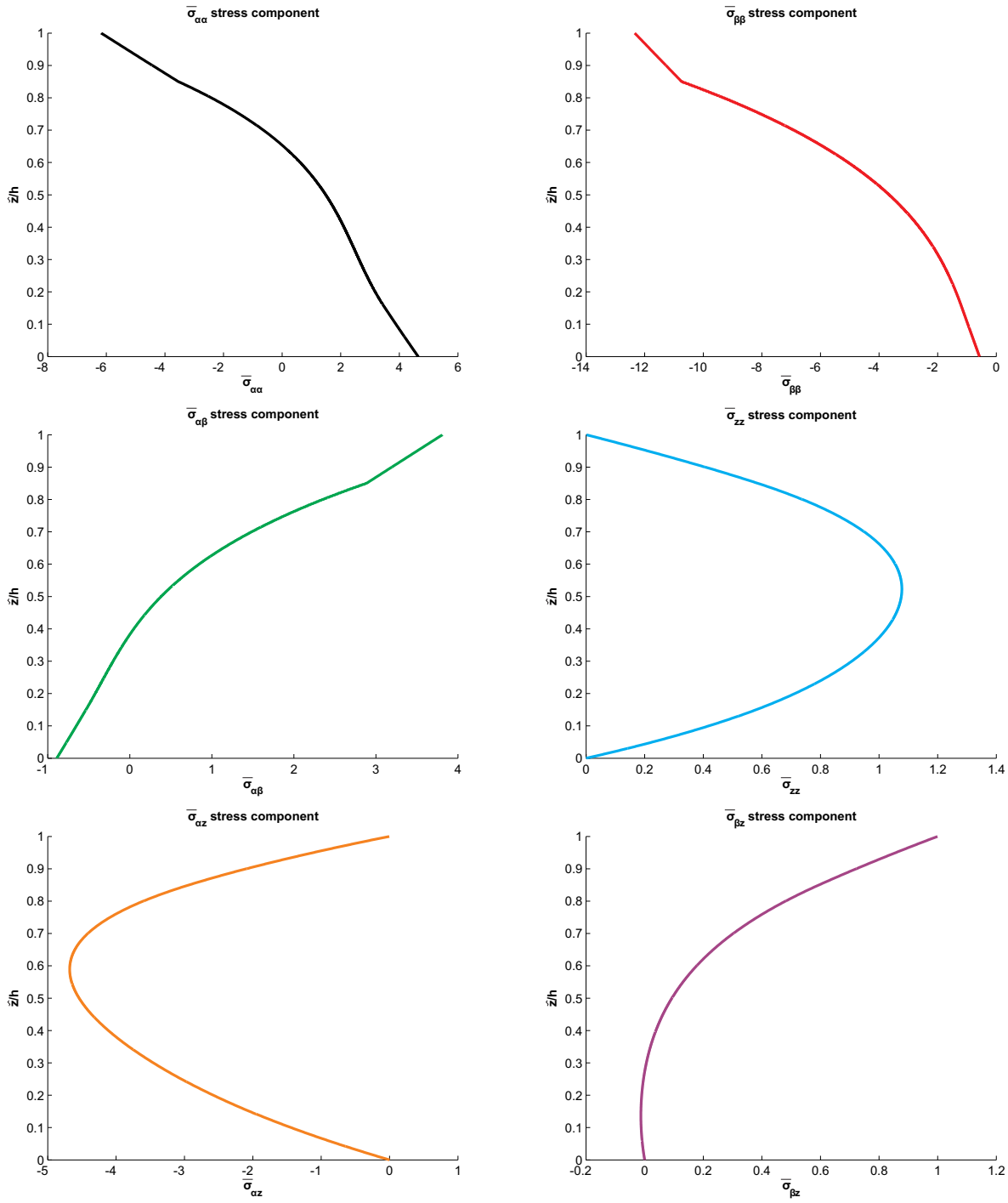

Figure 10: Benchmark 3, no-dimensional stresses through the thickness $\tilde{z}$ for $R_\alpha/h = 10$ and $p = 2.0$.

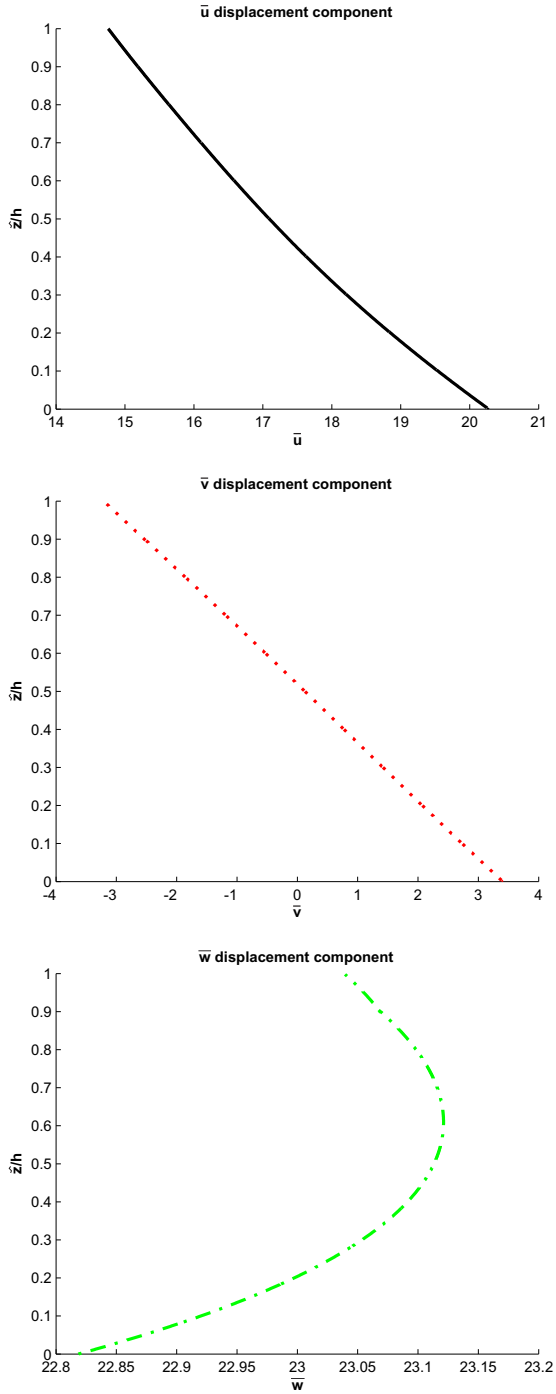

Figure 11: Benchmark 4, no-dimensional displacements through the thickness $\tilde{z}$ for $R_\alpha/h = 10$ and $p = 2.0$.

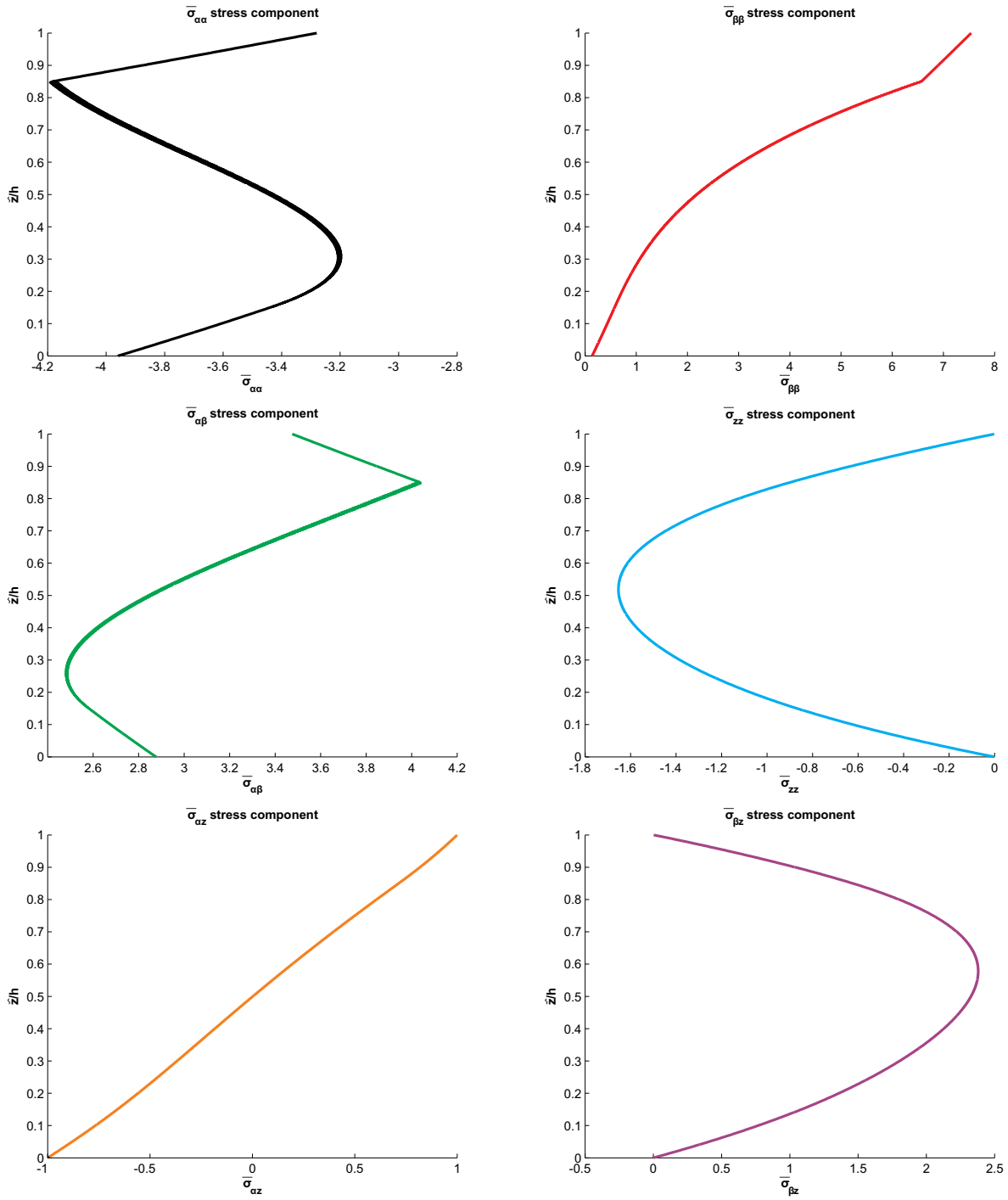

Figure 12: Benchmark 4, no-dimensional stresses through the thickness $\tilde{z}$ for $R_\alpha/h = 10$ and $p = 2.0$.